environmental microbiology

Environmental Microbiology (2021) **23**(11), 6463–6482 doi:10.1111/1462-2920.15794

Highly integrated adaptive mechanisms in *Spiribacter halalkaliphilus*, a bacterium abundant in Chinese soda-saline lakes

Qiong Xue,[1,2†] Dahe Zhao ,[1*†] Shengjie Zhang,[1,2] Heng Zhou,[1] Zhenqiang Zuo,[1,2] Jian Zhou,[1] Ming Li[1] and Hua Xiang[1,2*]

[1]*State Key Laboratory of Microbial Resources, Institute of Microbiology, Chinese Academy of Sciences, Beijing 100101, China.*

[2]*University of Chinese Academy of Sciences, Beijing 100049, China.*

Summary

Soda-saline lakes are polyextreme environments inhabited by many haloalkaliphiles, including one of the most abundant *Spiribacter* species. However, its mechanisms of adaptation are not ecophysiologically characterized. Based on a large-scale cultivation strategy, we obtained a representative isolate of this *Spiribacter* species whose relative abundance was the highest (up to 15.63%) in a wide range of salinities in the soda-saline lakes in Inner Mongolia, China. This species is a chemoorganoheterotrophic haloalkaliphile. It has a small and streamlined genome and utilizes a wide variety of compatible solutes to resist osmotic pressure and multiple monovalent cation/proton antiporters for pH homeostasis. In addition to growth enhancement by light under microaerobic conditions, cell growth, organic substrate consumption and polyhydroxybutyrate biosynthesis were also improved by inorganic sulfide. Both quantitative RT-PCR and enzymatic assays verified that sulfide:quinone oxidoreductase was upregulated during this process. Metatranscriptomic analysis indicated that all genes related to environmental adaptation were transcribed in natural environments. Overall, this study has identified a novel abundant haloalkaliphile with multiple and highly integrated adaptive strategies and found that inorganic sulfide was able to improve the adaptation of a heterotroph to polyextreme environments.

Received 21 July, 2021; revised 23 September, 2021; accepted 27 September, 2021. *For correspondence. E-mail xiangh@im.ac.cn; Tel. +86-10-64807472; Fax +86-10-64807472. E-mail zhaodh@im.ac.cn. †These authors have contributed equally to this work.

Introduction

Soda lakes are widely distributed in subtropical latitudes and rain-shadow zones in the continental interiors (Grant and Sorokin, 2011). In these double-extreme ecosystems, the total salinity usually ranges from approximately 5% (wt./vol.) to more than 30% (wt./vol.), while the pH value is usually higher than 9 and even approaches ~12 in some saturated lakes (such as Lake Magadi with >30% total salts described by Grant and Sorokin, 2011), which can be attributed to the high concentrations of carbonate/bicarbonate (Grant and Sorokin, 2011; Boros and Kolpakova, 2018). According to the latest definition, soda brines are classified into 'soda' and 'soda-saline' types. Unlike normal soda lakes, the chloride concentration is usually higher than that of carbonate/bicarbonate in soda-saline lakes (Boros and Kolpakova, 2018).

Soda lakes have surprisingly high biodiversity and abundant microbial resources (Lanzén *et al*., 2013; Vavourakis *et al*., 2016). To date, several microorganisms involved in elemental cycling, such as oxygenic photosynthetic cyanobacteria (Mikhodyuk *et al*., 2008), anoxygenic phototrophic bacteria (Gorlenko *et al*., 2009; Asao *et al*., 2011), degraders (Sorokin *et al*., 2019), sulfur-oxidizing bacteria (Sorokin *et al*., 2001), arsenite-oxidizing bacteria (Hoeft *et al*., 2007), methanogenic archaea (Sorokin *et al*., 2017), sulfate and elemental sulfur respiration bacteria (Sorokin *et al*., 2008; Sorokin *et al*., 2011) and archaea (Sorokin *et al*., 2016), have been obtained from soda lakes. In recent years, many more uncultured microbial taxa have been identified in soda and soda-saline lakes using high-throughput sequencing technology, many of which have shown potential for important biogeochemical functions, including some Actinobacteria members encoding the key enzymes of the Wood–Ljungdahl pathway for carbon fixation and dissimilation (Vavourakis *et al*., 2016; Vavourakis *et al*., 2018; Zhao *et al*., 2020). In addition, metatranscriptomic and metaproteomic studies have

been conducted to demonstrate microbial activities in natural environments (Edwardson and Hollibaugh, 2017; Vavourakis *et al*., 2019; Zorz *et al*., 2019).

The microorganisms inhabiting soda lakes usually prefer or depend on saline and alkaline environments and employ many strategies to adapt to the extreme environmental conditions. It has been reported that most haloalkaliphilic bacteria are able to synthesize or import compatible solutes (such as ectoine and glycine betaine) to achieve the osmotic balance, while the archaeal class *Halobacteria*, the bacterial order *Halanaerobiales*, and the bacterial genus *Salinibacter* accumulate inorganic salts (such as KCl) to maintain the high osmotic pressure inside the cell (Oren *et al*., 2002; Gunde-Cimerman *et al*., 2018). Monovalent cation/proton antiporters are usually involved in pH homeostasis in the cytosol, and Na^+/H^+-antiporters of the Nha family (Krulwich *et al*., 2011), or multisubunit Na^+/H^+ antiporter (named Mnh) of Mrp (multiple resistance and pH adaptations)-type (Ito *et al*., 1999), play a major role in microbial survival in high pH environments (Banciu and Muntyan, 2015). As haloalkaliphiles (live in saline–alkaline lakes and usually require high concentrations of chloride salts) and natronophiles (able to grow in nearly pure sodium carbonate brines) expend substantial energy during these processes of adaptation to high salinity and high pH (Sorokin *et al*., 2015), the tactics of broadening the sources and reducing the expenditure would further enhance environmental adaptability. In comparison, haloarchaea and *Salinibacter* bacteria usually thrive under extremely high salinity because their 'salt-in' strategy consumes less energy (Banciu and Muntyan, 2015; Gunde-Cimerman *et al*., 2018). In addition, certain abundant microorganisms, such as the moderately halophilic bacterium *Spiribacter salinus* inhabiting salterns (López-Pérez *et al*., 2013) and the marine halophilic SAR11 group (Giovannoni, 2017), have reduced or streamlined genomes; reduced genomes may minimize the material costs of cellular replication (Giovannoni *et al*., 2005). Other abundant microbes may utilize additional energy sources. The abundant heterotrophic haloarchaeon *Haloquadratum* and the bacterium *Salinibacter* are thought to obtain additional energy from sunlight via rhodopsins (Oren and Hallsworth, 2014). Diverse rhodopsins have been detected in microorganisms thriving in hypersaline salterns and bays (Papke *et al*., 2003; Maresca *et al*., 2018), and light can stimulate the growth of some heterotrophs containing light-driven proton pumps (e.g. proteorhodopsin) by regulating the central metabolic pathways (Palovaara *et al*., 2014).

Lately, we reconstructed 385 draft genomes from 18 metagenomes of brines and sediments of the soda-saline lakes in Inner Mongolia, China and analysed the metabolic pathways of 38 abundant metagenome-assembled genomes (MAGs) including *Spiribacter* sp. GPB-6 (Zhao *et al*., 2020), which was identified as one of the most abundant bacteria in a wide range of salinities. This raised an important scientific question: what are the mechanisms by which *Spiribacter* species adapt so efficiently to soda-saline environments? In this study, we obtained a representative strain of this abundant species through large-scale microbial isolation from samples from the same environment. The environmental adaptive mechanisms of this haloalkaliphile were systemically elucidated by linking genomic analysis with physiological features. Genes involved in compatible solute accumulation and pH homeostasis were found in the compacted genome, and light was able to enhance growth under microaerobic conditions. Interestingly, organic carbon utilization and cell growth were accelerated by the addition of sulfide to the growth media. These findings revealed the highly integrated adaptive strategies for this abundant species in soda-saline lakes; the multiple strategies were further supported with metatranscriptomic analysis.

Results

Isolation, phylogeny and relatedness indices of the Spiribacter *species*

To obtain pure cultures of the species of interest (including the abundant *Spiribacter* sp. GPB-6), a large-scale cultivation approach was used. A total of 25 media, including previously reported alkaline media AM, HM and M9; neutral media CM and NOM3; and the physiochemical parameter simulation media (PSM) LN, LH, ME, SB and TS were used to isolate as many microbes as possible from the 141 samples collected from 55 ponds of different salinities, which were naturally or artificially separated within the soda-saline lakes in Inner Mongolia, China. The information on the samples and the composition of the media are shown in Tables S1 and S2 respectively. In summary, 1302 pure strains were obtained, and their culture conditions and habitats, together with the taxonomic classification based on the 16S rRNA genes, are shown in Table S3. Strain collection is illustrated in Fig. S1 and isolate IM2438^T as a representative strain of GPB-6 was included (described below and in the Supplementary Results).

The full-length 16S rRNA gene (locus tag GJ672_08480 in GenBank) from the genome of IM2438^T was confirmed using Sanger sequencing (MN713357 in Table S3), which shared 100% identity with the 16S rRNA gene fragment of GPB-6 (Table S4 and details are described in the Supplementary Results). In the

phylogenetic tree of the 16S rRNA genes, isolate IM2438^T and MAG GPB-6 clades were separated from the other related species (Fig. S2). The identity of the IM2438^T 16S rRNA gene and the most closely related species (*Spiribacter salinus* M19-40^T) was 98.43% (Tables S3 and S5), which was lower than the novel species threshold (98.7%) (Kim *et al*., 2014). Furthermore, the phylogenomic tree based on 120 ubiquitous bacterial single-copy genes also supported that isolate IM2438^T and MAG GPB-6 cluster in a clade with MAG T1Sed10_76, another *Spiribacter* MAG, but not abundant in the metagenomes of the sediments of Siberian soda lakes (Vavourakis *et al*., 2018), and they represented a novel species-level lineage of the *Spiribacter* genus with 99% bootstrap support (Fig. 1A).

Furthermore, a genome-based relatedness analysis was performed. Orthologous average nucleotide identity (OrthoANI) of isolate IM2438^T and MAG GPB-6 was 99.57%, and both genomes were closely related to T1Sed10_76 (97.74% and 98.15% respectively) (Fig. 1B). This confirmed that three genomes belong to one species according to the species boundary of 95% ANI (Jain *et al*., 2018). OrthoANI values with other *Spiribacter* species ranged from 72.56% to 74.11%. The genomic similarities among *Spiribacter* genomes were also calculated using ANIb [a BLAST-based average nucleotide identity (ANI)], ANIm (a Mummer-based average nucleotide identity) and Genome-to-Genome Distance Calculator (GGDC), and they were consistent with the results above (Table S6). Almost all fragments of GPB-6 were mapped to the genome of IM2438^T with high similarity (Fig. 1C). These results demonstrate that the isolate IM2438^T is a pure culturable representative of GPB-6 and represents a new species of the genus *Spiribacter*. Considering its relative abundance in natural environments and the optimum growth conditions in the laboratory, we proposed the name *Spiribacter halalkaliphilus* for this lineage (described below).

The species S. halalkaliphilus *is abundant in soda-saline lakes*

Our previous metagenomic investigation has shown that the *S. halalkaliphilus*-related MAGs GPB-6 was abundant in soda-saline lakes (Zhao *et al*., 2020), and the more detailed information is presented in supplementary materials and Fig. S1c. To verify these results, the reads mapped to the complete genome of the isolate IM2438^T were retrieved from the 18 metagenomes to quantify this abundant species (shown in Fig. 2A). The sample names, DK and HC, represent Habor Lake and Hutong Qagan Lake respectively, the number indicates the salinity, and S and W signify sediment and water (or brine) samples respectively. The related reads accounted for 15.63%, 8.40% and 7.94% of all clean reads in HC17W, HC22W and DK20W respectively, which were much higher than those of the other samples (Fig. 2A).

To provide more evidence, the raw reads mapped to the IM2438^T whole genome were also retrieved from the metatranscriptomes of four brine samples from the same region. The salinities of the four brine samples ranged from 3% to more than 32% (Table S7). The clean bases of the metatranscriptome ranged from 21 to 27 Gb, and the ratios of assigned fragments to the IM2438^T genome were as high as 29.6% and 14.6% in the samples with 15% and 22% salinity respectively (Fig. 2B), much higher than those at 3% and more than 32% salinity (no more than 0.1%). In a word, both metagenomic and metatranscriptomic analyses supported that IM2438^T was representative of an abundant species detected at least in some brines with a salinity of 15%–22%.

Chemoorganoheterotrophic lifestyle of S. halalkaliphilus

In the laboratory, the isolate IM2438^T was able to grow in a wide range from 3% to 27% (wt./vol.) total salinity with an optimum of 10%–11%, and at pH 8.0–11.0 with an optimum pH 9.0 (Fig. 3A and B). Carbon source utilization showed that only lactate, pyruvate and acetate could support growth and that cell growth was faster on lactate than on pyruvate or acetate (Fig. S6a). Therefore, we designed an optimal medium SH10 (salinity of 10%, pH of 9.0, and carbon source of lactate; the composition is shown in the Experimental Procedures) for IM2438^T. Cultured with lactate as a carbon source at 37°C, the colour of IM2438^T colonies on solid plates was light purple (Fig. 3C) and the cells were curved rods or short spirals with a size range of 0.2–0.3 μm (width) by 0.5–1.5 μm (length) (Fig. 3D and E).

In the genome of IM2438^T; *lldD*, *ldhA* and *dld* (three lactate dehydrogenase genes); *lctP* for lactate utilization; and *acyP*, *pta*, *acs* and *actP* for acetate utilization; were found (Fig. 4A). To investigate whether these genes are functional in natural environments, the transcription activity of each gene was analysed based on the environmental metatranscriptomes and normalized to transcripts per million (TPM). The genes involved in lactate, pyruvate and acetate transportation and utilization were all highly transcribed (Fig. 4B), indicating that these three organic acids could also be utilized for survival in natural environments. The citrate cycle and oxidative phosphorylation were observed for anabolism and energy metabolism (Fig. 4 and Table S8). As IM2438^T was able to grow under aerobic conditions with the addition of a carbon source but was unable to perform anaerobic and autotrophic growth (data not shown), it is an aerobic chemoorganoheterotrophic microbe.

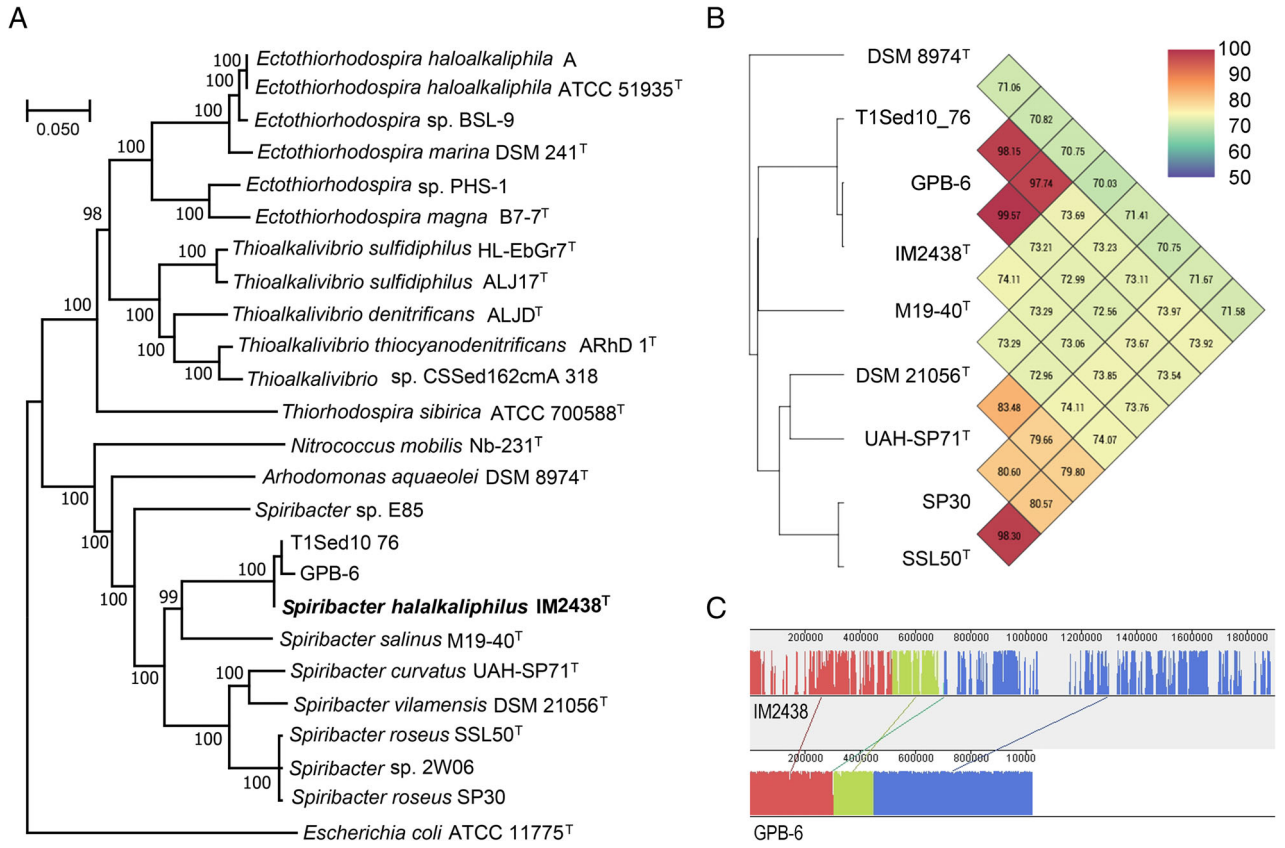

Fig. 1. Phylogeny and relatedness analysis of *S. halalkaliphilus* IM2438^T.
A. Phylogenomic tree based on concatenated amino acid sequences of 120 ubiquitous single-copy proteins. There are 5040 columns in the amino acid multiple sequence alignment extracted from the output of GTDB-Tk. Bootstrap values (%) were based on 1000 replicates, and those with over 70% bootstrap support are shown. Bar, 0.05 substitutions per amino acid position.
B. Average nucleotide identity matrix at the genome level. The phylogenetic tree was constructed based on ANI distances using OrthoANI. The strain names are the same as in subgraph A.
C. Genome-wide alignment of IM2438^T and GBP-6 using the Mauve software. The GPB-6 genome was rearranged by referring to that of IM2438^T, and the similarity plot and locally collinear blocks are exhibited. GenBank accession numbers of genomes: *Thioalkalivibrio thiocyanodenitrificans* ARhD 1^T (AQZO00000000); *Thioalkalivibrio* sp. CSSed162cmA 318 (SKOF00000000); *Thioalkalivibrio denitrificans* ALJD^T (MVBK00000000); *Thioalkalivibrio sulfidiphilus* HL-EbGr7^T (CP001339); *Thioalkalivibrio sulfidiphilus* ALJ17 (ARJH00000000); *Thiorhodospira sibirica* ATCC 700588^T (AGFD00000000); *Ectothiorhodospira* sp. PHS-1 (AGBG00000000); *Ectothiorhodospira magna* B7-7^T (FOFO00000000); *Ectothiorhodospira marina* DSM 241^T (FOAA00000000); *Ectothiorhodospira* sp. BSL-9 (CP011994); *Ectothiorhodospira haloalkaliphila* A (CP007268); *Ectothiorhodospira haloalkaliphila* ATCC 51935^T (AJUE00000000); *Nitrococcus mobilis* Nb-231^T (AAOF00000000); *Arhodomonas aquaeolei* DSM 8974^T (ARGF00000000); *Spiribacter* sp. E85 (QFFI00000000); *Spiribacter salinus* M19-40^T (CP005963); *Spiribacter halalkaliphilus* IM2438^T (CP046046); T1Sed10 76 (PWEP00000000, a MAG from metagenomic investigation of Siberian soda lakes); GPB-6 [a MAG from metagenomic research of soda-saline lake in Inner Mongolia (Zhao *et al*., 2020)]; *Spiribacter* sp. 2W06 (MDVM00000000); *Spiribacter curvatus* UAH-SP71T (CP005990); *Spiribacter vilamensis* DSM 21056^T (SHLI00000000); *Spiribacter roseus* SSL50^T (CP016382); *Spiribacter roseus* SP30 (VMKP00000000); *Escherichia coli* ATCC 11775^T (CP033092).

Large inclusion granules were observed in the cytosol using transmission electron microscopy (TEM) (Fig. 3E), and gas chromatography indicated that polyhydroxybutyrate (PHB) was produced (Fig. 6C). The genes *ACAT* (encoding acetyl-CoA C-acetyltransferase), *phbB* (encoding acetoacetyl-CoA reductase) and *phaCE* (encoding polyhydroxyalkanoate synthase subunits PhaC and PhaE) for PHB synthesis were also annotated in the genome (Fig. 4A). The transcripts of these genes were detected in the four metatranscriptomes of the natural brine samples, and the transcriptional activity of two genes (*phaP_1* and *phaP_2*) annotated as phasin family proteins involved in the formation of PHB granules was extremely high (Fig. 4B). Thus, we inferred that *S. halalkaliphilus* may accumulate intracellular PHB as storage of carbon and energy in natural environments.

Adaptation mechanisms of S. halalkaliphilus *to double extreme conditions*

The molecular basis of bacterial adaptation to saline and alkaline conditions was elucidated based on the genome of IM2438^T and metatranscriptomes. The biosynthesis

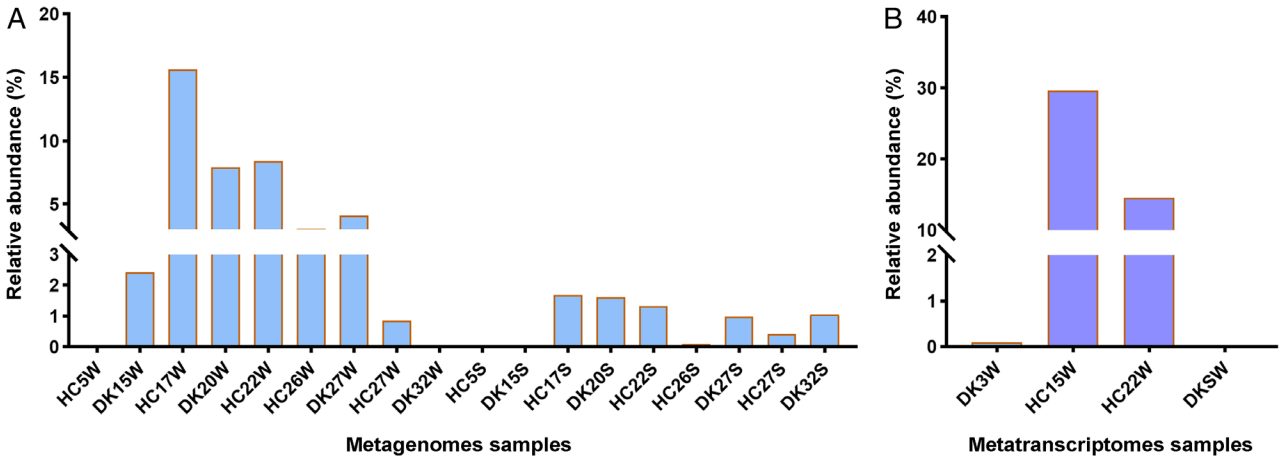

Fig. 2. Relative abundance of *S. halalkaliphilus* IM2438^T estimated through metagenomes and metatranscriptomes.
A. The percentage of the reads mapped to the complete genome of the IM2438^T in the 18 metagenomes (Zhao *et al*., 2020).
B. The percentages of reads mapped to the reversely stranded cDNA of each gene of the IM2438^T in the four metatranscriptomes.

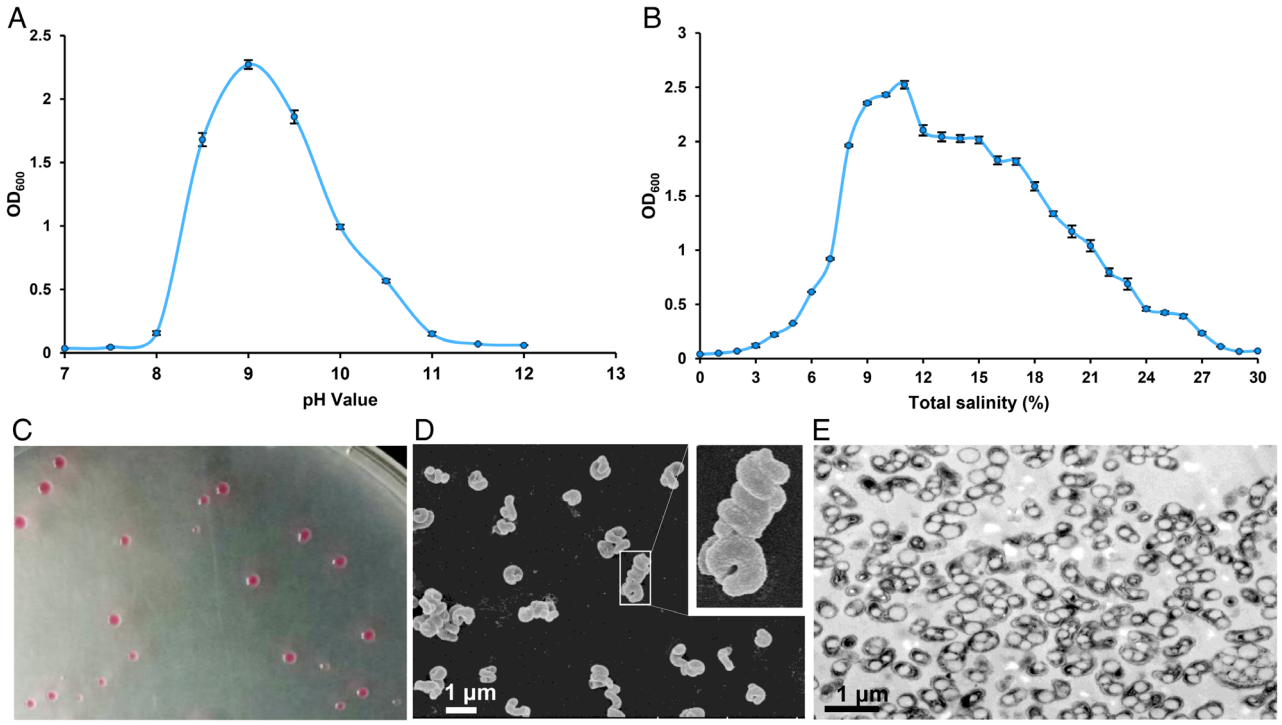

Fig. 3. Physiological and morphological characteristics of *S. halalkaliphilus* IM2438^T.
The effect of pH (A) and total salinity (B) on growth (cell concentration at 120 h) were estimated in liquid media. The pH value and total salinity varied based on SH10, with a pH of 9 and a total salinity of 10%. The cultures were incubated at 37°C with shaking at 200 rpm. The data (A, B) are the mean values and standard deviations from two parallel incubations.
C. Colony morphology on the SH10 plate (approximately 72 h).
D. Observation of cell morphology using scanning electron microscopy (SEM).
E. Observation of PHB granules using transmission electron microscopy (TEM). Cells were collected from the liquid culture in the SH10 medium at the exponential phase for SEM and TEM observations. Bar, 1 μm (D, E).

and import of compatible solutes involved in adaptation to high salinity were analysed. Three marker genes for ectoine synthesis (*ectB* encoding diaminobutyric acid aminotransferase, *ectA* encoding diaminobutyric acid acetyltransferase and *ectC* encoding ectoine synthase), two for glycine betaine (*betA* encoding choline

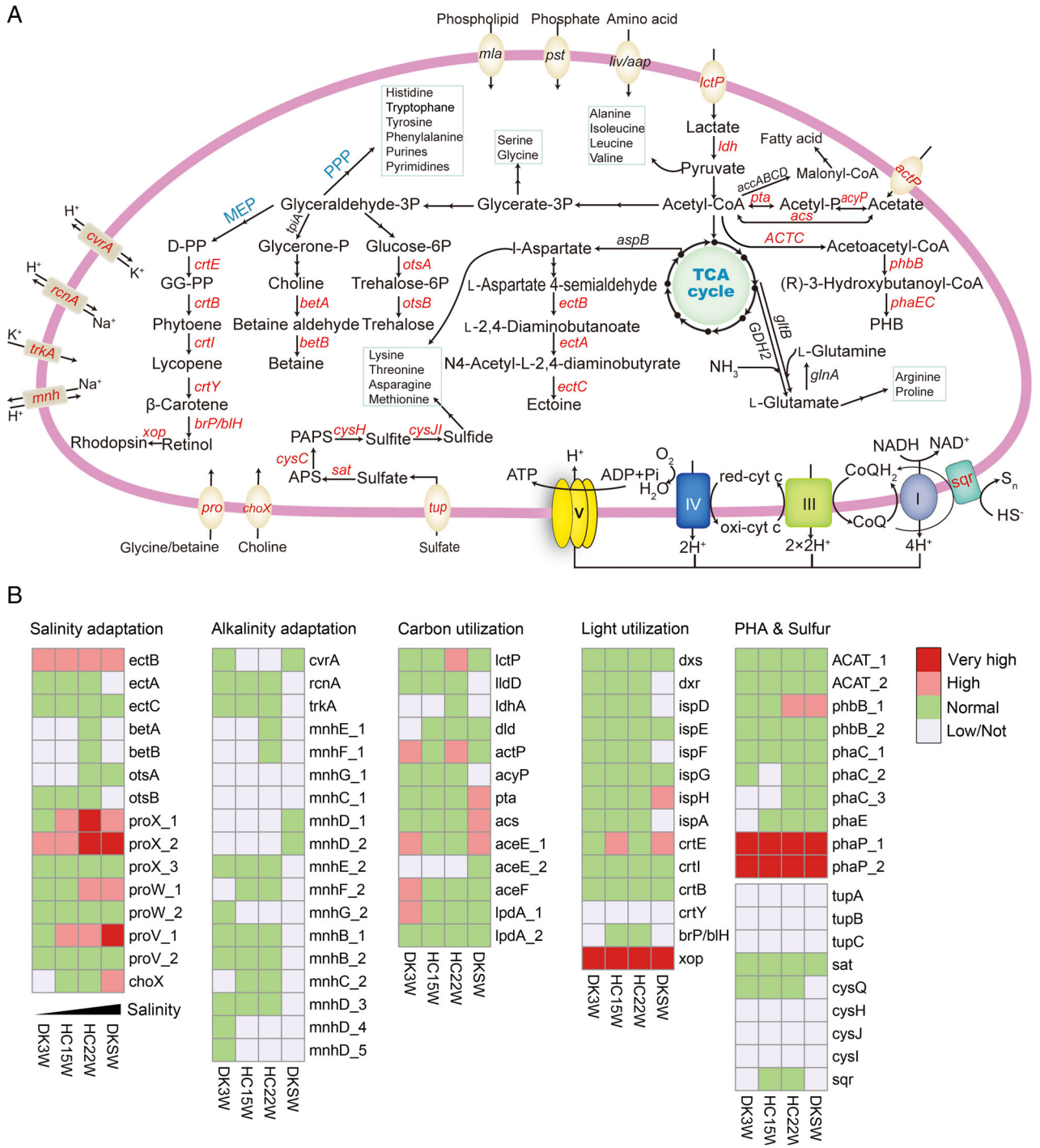

Fig. 4. Metabolic pathways and relative metatranscriptomic activity of *S. halalkaliphilus* IM2438^T.

A. Reconstruction of metabolic pathways based on the genome annotation. Abbreviations: MEP, methylerythritol phosphate pathway; PPP, pentose phosphate pathway; TCA cycle, tricarboxylic acid cycle; Acetyl-P, acetyl-phosphate; Glycerate-3P, glycerate-3-phosphate; Glyceraldehyde-3P, glyceraldehyde-3-phosphate; D-PP, dimethylallyl diphosphate; GG-PP, geranylgeranyl diphosphate; Glycerone-P, glycerone-phosphate; Glucose-6P, glucose-6-phosphate; Trehalose-6P, trehalose-6-phosphate; PAPS, 3′-phosphoadenosine 5′-phosphosulfate; APS, adenosine 5′-phosphosulfate; PHB, polyhydroxybutyrate; and red-cyt *c*/oxi-cyt *c*, reduced/oxidized form of cytochrome *c*; enzyme names of key genes are shown in Supplementary Table S8.

B. Relative metatranscriptomic activity of key genes in four samples with various salinities. Transcription activity was expressed as transcripts per million (TPM) and grouped using the percentage ratio of TPM to the average transcripts per million (ATPM): very high, >500%; high, 200%–500%; normal, 20%–200%; and low/not, <20%.

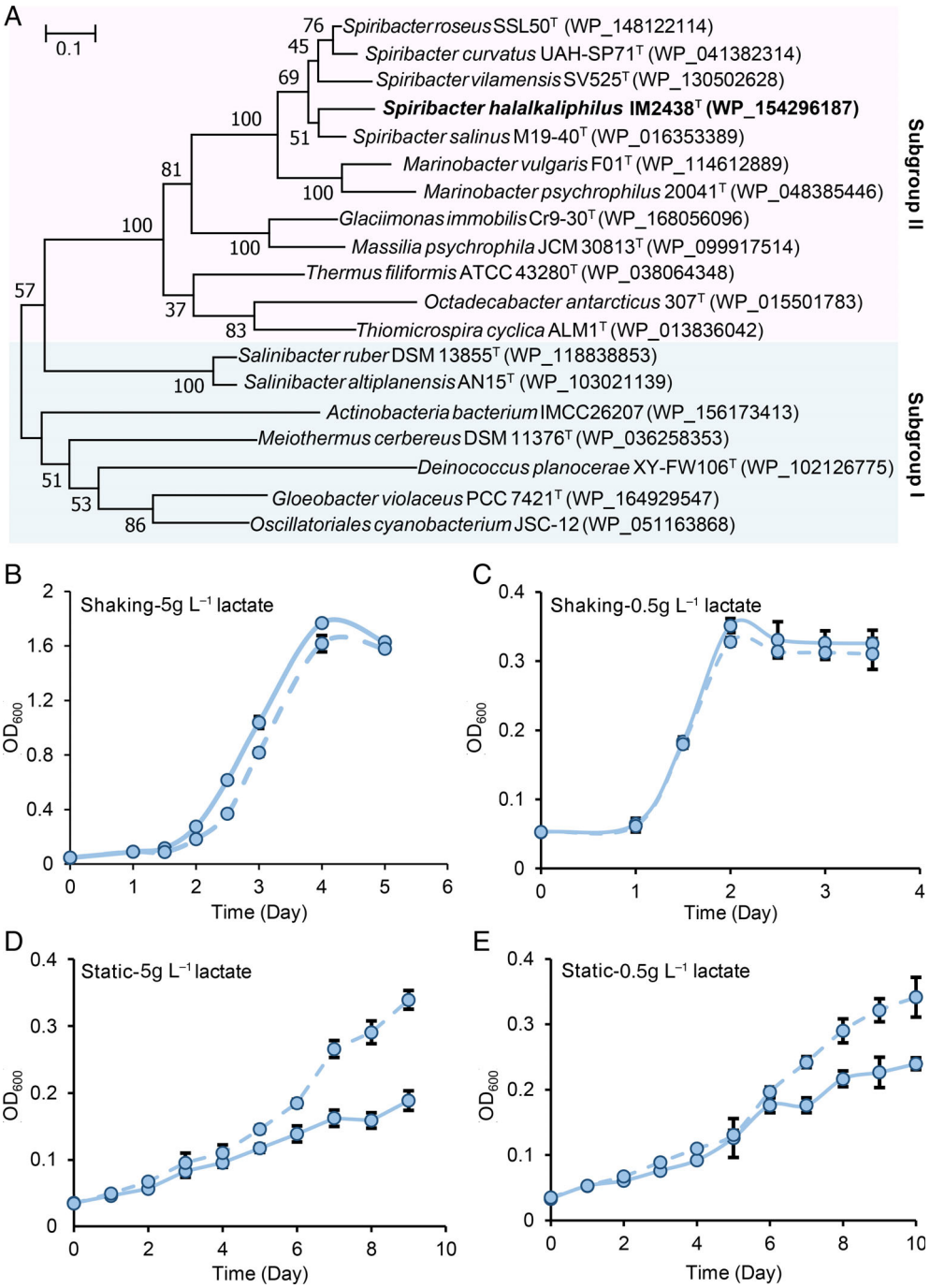

Fig. 5. Phylogenetic analysis of xanthorhodopsin-encoding gene and influence of light on cell growth.
A. Maximum-likelihood phylogenetic tree based on the amino acid sequence of xanthorhodopsin from *S. halalkaliphilus* IM2438^T. The labels at each leaf are species names and accession numbers in the GenBank.
B–E. Growth curve of IM2438^T with different substrate concentrations and culture conditions. The cell concentration was estimated by measuring the optical density at 600 nm. The dashed and solid lines represent the culture conditions with and without light respectively. The medium was (or based on) SH10, and the lactate concentration was 5 g L^{-1} (B, D) or 0.5 g L^{-1} (C, E). Aerobic and microaerobic cultivations were respectively performed by shaking at 200 rpm (in flasks) and by static cultivation (the volume ratio of air to medium was 1:1 in screw-capped bottles). The data are the mean values and standard deviations from three parallel incubations.

dehydrogenase and *betB* encoding glycine betaine aldehyde dehydrogenase) and two for trehalose (*otsA* encoding trehalose 6-phosphate synthase and *otsB* encoding trehalose 6-phosphate phosphatase) were annotated (Fig. 4A; Table S8). In addition, ABC-type betaine transporter genes, *proXWY*, and choline

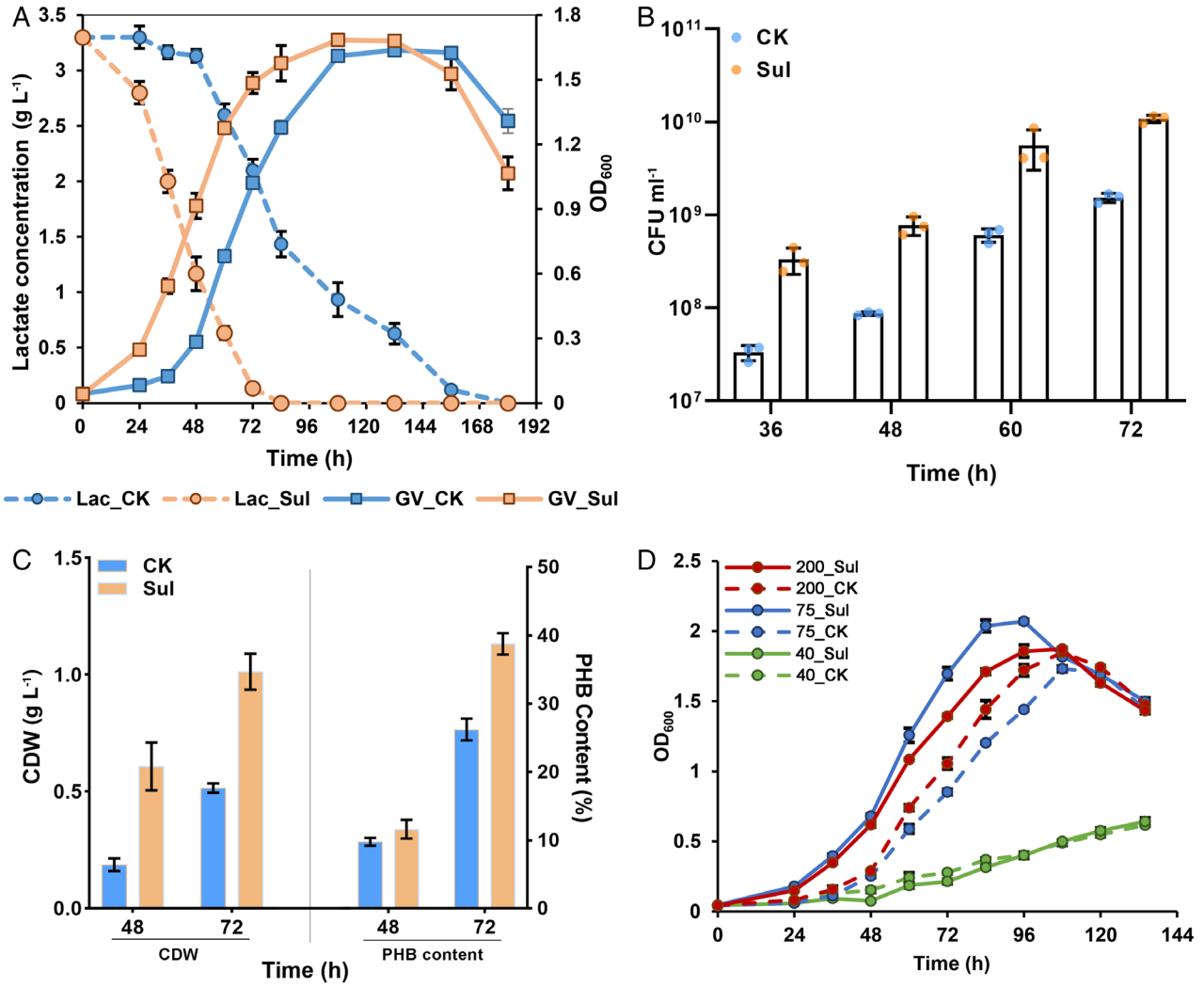

Fig. 6. Influence of sulfide on the growth and metabolism of *S. halalkaliphilus* IM2438^T.
A. Time course of cell growth and lactate consumption by *S. halalkaliphilus* IM2438^T in SH10 medium. The circle dots and dashed lines represent the residual lactate concentration (Lac), and the square dots and solid lines represent the growth curve (GV) estimated at an optical density at 600 nm. The orange and blue lines represent the experimental group with sulfide (Sul) and the negative control group without sulfide (CK) respectively. The sulfide concentration was 15 mM. The cultures were incubated with 200 rpm shaking.
B. The cell numbers at various phases counted on SH10 plates. The time point was coincident with subgraph (A).
C. Influence of sulfide on CDW and PHB content. PHB content is the percentage of PHB mass in the CDW.
D. Growth curve of IM2438^T with or without sulfide in SH10 medium at different shaking speeds of 200, 75 and 40 rpm. All the data are the mean values and standard deviations from three parallel incubations.

transporter gene, *choX*, were also found. Transcripts of almost all genes involved in ectoine and trehalose biosynthesis and those of the glycine betaine transporter genes were detected in the metatranscriptomes of four natural brine samples, and a glycine betaine transporter operon (*proX_1*, *proW_1* and *ProV_1*) exhibited greater transcriptional activity at higher salinities (Fig. 4B; Table S8). Consequently, ectoine, glycine betaine and trehalose may accumulate by *S. halalkaliphilus* to balance the extracellular osmotic pressure. Comparison of transcriptional activity between different salinities (HC15W and HC22W) indicated that the gene transcripts for glycine betaine synthesis and transportation were greater in the more saline brine (Fig. 4B; Table S8), suggesting that glycine betaine was the main contributor to the response to high salinity. The proteomic isoelectric point profile of IM2438^T was similar to that of *Halomonas ventosae* but different from that of *Haloferax mediterranei*, suggesting that the salt-in strategy may not be adopted (Fig. S3).

The genes involved in adaptation to alkalinity were also analysed. The Nha family potassium/proton antiporter gene *nhaP2* and two copies of multicomponent Na^+:H^+ antiporter operons were predicted to function in pH

homeostasis in *S. halalkaliphilus* (Table S9). Almost all transcripts of the abovementioned genes were observed (Fig. 4B; Table S8), indicating their function in natural environments. In some alkaliphiles, alternative sodium motive force is generated for ATP synthesis to cope with the low availability of proton (Hicks *et al*., 2010; Banciu and Muntyan, 2015). In the genome of *S. halalkaliphilus*, however, none of Na^+-translocating NADH:ubiquinone oxidoreductase (Na^+-NQR), Na^+-translocating ferredoxin:NAD^+ oxidoreductase (Rnf) and Na^+ extruding oxaloacetate decarboxylase (OadA) was annotated, and all 14 subunits of H^+-translocating NADH:ubiquinone oxidoreductase (Nuo) were found (Table S8). The amino acid residues Gln^{32}, Val^{63}, Glu^{65} and Ser^{66} of the rotor ring (*c*-subunit) of Na^+-translocating F_1F_0-ATP synthase were involved in the binding and translocation of sodium ion, and some residues were identified through mutation (Kaim *et al*., 1997; Meier *et al*., 2005). Similarly, none of these residues was present in the ATPase of *S. halalkaliphilus* (Fig. S4). These results indicated that H^+-coupled ATP synthesis, but not Na^+-coupled ATP synthesis, was adopted by *S. halalkaliphilus*.

The genome of isolate IM2438^T is small and compact, with only 1 900 931 bp in size, similar to other members of *Spiribacter* but much smaller than those of closely related genera, and the median length of intergenic regions is also shorter (Fig. S5).

Utilization of light energy by S. halalkaliphilus *under microaerobic conditions*

In the genome of IM2438^T, a light-driven proton pump xanthorhodopsin gene (abbreviated *xop* in this article) was identified, and a complete methylerythritol phosphate (MEP) pathway (for terpenoid backbone biosynthesis) and a retinal biosynthesis pathway were annotated (Fig. 4A; Table S8). Sequence similarity analysis showed that xanthorhodopsin from IM2438^T was closely related to that from *S. salinus* M19-40^T (with 83.73% identity) and they belonged to subgroup II (Fig. 5A). In the metatranscriptomes, the transcripts of genes in the MEP and retinal biosynthesis pathways were detected in most samples, except for under more than 32% salinity (Table S8). In addition, *xop* was transcribed very highly (Fig. 4B), and the TPM values of the xanthorhodopsin gene exceeded 10 000, which was much higher than that of the other genes. This suggests that when light is available in natural environments, the xanthorhodopsin pathway may function as an additional energy source to support growth.

To validate the function of xanthorhodopsin in microbial adaptability, we compared the growth of IM2438^T under light and dark conditions. The initial results showed that light did not enhance cell growth in the optimal SH10 medium (Fig. 5B). Therefore, the culture conditions for xanthorhodopsin function were further explored; however, varying carbon sources (pyruvate or acetate) and increasing salinity both failed to stimulate xanthorhodopsin function (Fig. S6b, c and d), and no growth advantage under light was observed at a low carbon source concentration (Fig. 5C). Finally, we conducted static culture of this bacterium in SH10 medium and found that light could significantly increase cell growth (Fig. 5D and E). These results demonstrate that *S. halalkaliphilus* can utilize light energy under microaerobic conditions.

Sulfide promotes cell growth and carbon metabolism of S. halalkaliphilus

To determine the effects of sulfide on the cell growth of IM 2438, the time course of turbidity (OD_{600}) and residual lactate concentration were investigated. The results showed that the strain started to grow in less than 24 h in SH10 medium and that the maximum OD_{600} was approximately 1.6. When sulfide was added, the strain started to grow before 24 h, and the OD_{600} values were all greater than those of the control group without sulfide (Fig. 6A); correspondingly, substrate consumption was also stimulated. Lactate concentration started to decrease at 48 h and almost reached zero at 180 h in the absence of sulfide, while in the medium with sulfide added, the lactate concentration decreased sharply before 24 h to zero at 84 h (Fig. 6A). Cell growth and lactate consumption were slower under 20% salinity than under optimum salinity (10%); however, they could also be enhanced by adding sulfide (Fig. S7).

To verify the effect of sulfide on cell growth, cell number was quantified using the plate count method. The culture was diluted and then spread on the SH10 plate to ensure that the number of single colonies was counted. The results showed that there were $3.2 \times 10^7 \pm 0.6 \times 10^7$ colony forming units (CFUs) per millilitre at 36 h without sulfide, while $3.4 \times 10^8 \pm 1.0 \times 10^8$ CFUs ml^{-1} was observed when sulfide was added (Fig. 6B), a 9.5-times increase. At 48, 60 and 72 h, the addition of sulfide also increased the CFUs by 8.3, 7.5 and 6.1 times respectively (Fig. 6B). The effects of sulfide on cell dry weight (CDW) and PHB accumulation were further investigated, and the cells were collected to quantify CDW and PHB mass (Fig. 6C). At 48 h, the average CDW was 0.2 ± 0.0 g L^{-1} in the control group and increased to 0.6 ± 0.1 g L^{-1} with the addition of sulfide. The PHB content also improved from 9.8% in the control group to 11.6% in the sulfide group. At 72 h, both CDW and PHB contents were much greater when sulfide was added. CDW increased approximately twice, while PHB content increased more than 1.5 times.

The effect of sulfide on dissolved oxygen should be considered; however, the oxygen concentration is difficult to determine because it varies during growth; therefore, we tested the influence of sulfide on cell growth under different shaking speeds. The results showed that IM2438^T grew fastest with shaking at 200 rpm (more oxygen) but more slowly when the shaking speed decreased (75 and 40 rpm, less oxygen) when sulfide was not added (Fig. 6D). This corresponded with the obligate aerobic characteristics. After adding sulfide, cell growth could also be improved under microaerobic conditions of 75 rpm shaking but not under the condition of 40 rpm shaking (Fig. 6D). Remarkably, the extent of improvement under shaking at 75 rpm was higher than that at 200 rpm. The culture conditions of adding sulfide and reducing shaking speed could give rise to a low oxygen concentration but lead to opposite effects on growth (Fig. 6D). Thus, the growth promotion by the addition of sulfide was not because of the hypoxic environment caused by sulfide.

SQR was upregulated by sulfide

To decipher the molecular mechanism of sulfide on cell growth and metabolism in this heterotroph, we analysed the putative functional genes. *sqr* (encoding SQR) was annotated in the genome of IM2438^T and SQR-catalysed sulfide oxidation and transferred electrons to quinone (Fig. 4A). SQR enzymes were categorized into six groups (Marcia *et al*., 2010), and SQR from IM2438^T (GJ672_07015) was located in the type II branch (Figs 7A and S8). This SQR consists of 442 amino acids and contains the conserved amino acid residues K312, C350 and K397 based on the protein structure of V_Aam SQR (Fig. 7B). One transmembrane region was predicted at 13–35 amino acids (Fig. S9); meanwhile, a twin-arginine translocation signal peptide of 39 amino acids in length was predicted with a likelihood of 0.9994, and a cleavage site between amino acids 40 and 41 was predicted with a probability of 0.9361 (Fig. S10).

The transcription activity of *sqr* was determined using quantitative reverse transcription-PCR (qRT-PCR). Compared with the control (no sulfide added to the culture medium), the levels of *sqr* transcript increased to 5.7 times when sulfide was added (Fig. 7C). This result indicated that *sqr* was transcribed and upregulated when sulfide was present in the culture. Similarly, the transcription activity of the PHB biosynthesis gene cluster (*rbs-phaC-phaE*) was upregulated 2.8-fold and another class I *phaC* (named *phaC* I) was upregulated 1.7-fold when sulfide was added (Fig. 7C). On the contrary, *cit* (encoding citrate synthase functions in the first step of the citrate cycle) was downregulated to 37% (Fig. 7C).

To compare the differences in the enzymatic activity of SQR, the cells were collected from the cultures with or without sulfide, and then the activity of sulfide oxidation was measured. In this assay, the maximum sulfide oxidation rate occurred in the first 5 min. Approximately 0.37 mM sulfide was oxidized by the cells that were collected from the culture with sulfide (Sul, orange line in Fig. 7D), whereas only 0.12 mM sulfide was oxidized by the same number of cells that were collected from the culture without sulfide (CK, blue line in Fig. 7D). To further estimate abiotic oxidation, the cells cultured with sulfide addition were heat-killed by boiling for 10 min. The sulfide degradation curve of these cells (Sul-Boiling, Fig. 7D) was almost the same as that of cells cultured without sulfide. The results indicated that sulfide oxidation activity was present in the cells cultured with sulfide, while no biological oxidation activity was detected in the control (no sulfide addition during cell culture), and that SQR may function in sulfide oxidation. In addition, transcripts of *sqr* were also detected in the metatranscriptomes of HC15W and HC22W (Fig. 4B), indicating the sulfide oxidation activity of IM2438^T in the natural environment.

Discussion

The abundant species *S*. *halalkaliphilus* IM2438^T is an ideal model bacterium for research on adaptation mechanisms in polyextreme environments. Similar to the neutral *S*. *salina* abundant in salterns (López-Pérez *et al*., 2013), *S*. *halalkaliphilus* has a relatively small genome size and short intergenic regions (Fig. S5). This was, in part, related to consistent selection of streamlined genome across the evolutionary history of the genus *Spiribacter*, similar to SAR11 (Giovannoni, 2017), which was subjected to environmental selection to minimize the material costs of cellular replication (Giovannoni *et al*., 2005). In addition, physiological properties and metabolic capabilities may also be subject to the powerful selection by double-extreme environments of soda-saline lakes. In contrast to the neutral counterparts in *Spiribacter*, two copies of multicomponent Na^+:H^+ antiporter genes were annotated in the genome of *S*. *halalkaliphilus* (Table S9). This transporter system plays an essential role in the physiology of alkaliphilic *Bacillus* (Swartz *et al*., 2005), and the double copy number makes the maintenance of pH more feasible. Similarly, alkaliphilic *Natranaerobius thermophilus* utilizes at least eight electrogenic $Na^+(K^+)$/H^+ antiporters for cytoplasm acidification at extracellular pH values at and below the optimum pH of 9.5 (Mesbah *et al*., 2009). Some alkaliphiles adopt Na^+-coupled oxidative phosphorylation for ATP synthesis (Banciu and Muntyan, 2015), but *S*. *halalkaliphilus* may retain the

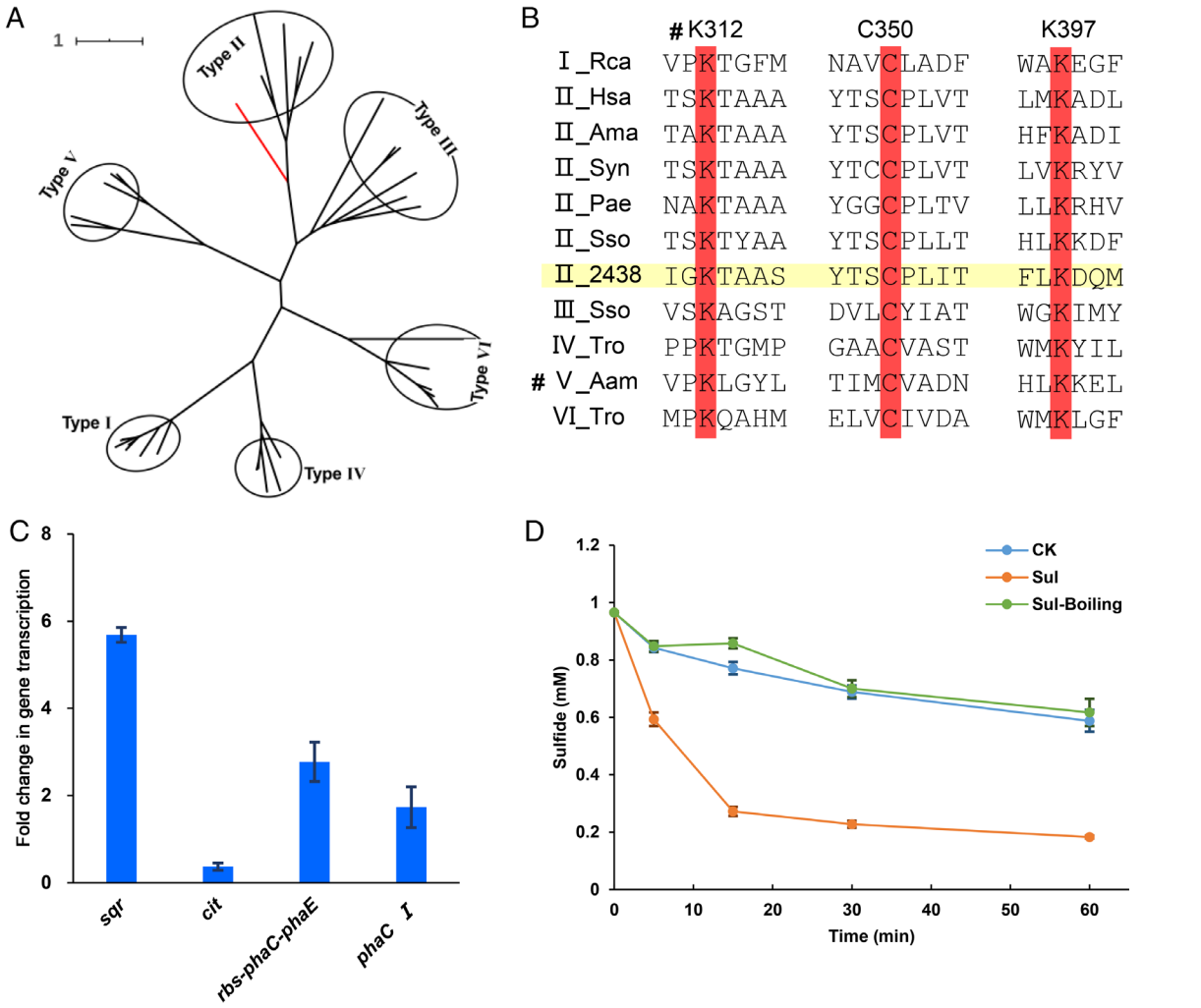

Fig. 7. Bioinformatics analysis, transcription regulation and enzymatic assay of sulfide:quinone oxidoreductase (SQR).
A. Unrooted maximum-likelihood tree based on the amino acid sequences of SQR. The red branch is the SQR of IM2438^T. The detail is shown in Fig. S8.
B. Alignment of amino acid sequences of SQR. The conserved amino acid residue sites are indicated by a red background, and the positions (K312, C350 and K397) at V_Aam are labelled #. The sequence of IM2438^T is indicated by a yellow background. The bacterial sources and accession numbers of SQR: I_Rca, *Rhodobacter capsulatus* DSM1155 (CAA66112); II_Hsa, *Homo sapiens* (NP067022); II_Ama, *Arenicola marina* (ABV22505); II_Syn, *Synechocystis* sp. PCC6803 (np440916); II_Pae, *Pseudomonas aeruginosa* (WP_003089452); II_Sso, *Schizosaccharomyces pombe* 927h- (NP_596067); II_2438, *Spiribacter halalkaliphilus* IM2438^T (GJ672_07015); III_Sso, *Saccharolobus solfataricus* P2 (sso2629); IV_Tro, *Thiocapsa roseopersicina* BBS (ASA46428); V_Aam, *Acidianus ambivalens* DSM 3772 (CAD33806); VI_Tro, *Thiocapsa roseopersicina* BBS (ASA46433).
C. Transcription regulation of *sqr* and related genes by sulfide was determined using qRT-PCR. The fold change was calculated using the Delta–Delta Ct method, and the formula used was $2^{[-((Ct_{interest} - Ct_{16S})_{Sul} - (Ct_{interest} - Ct_{16S})_{CK})]}$. In this formula, $Ct_{interest}$ and Ct_{16S} indicate the Ct values of the cDNA of interest and 16S rRNA respectively, while Sul and CK indicate the ΔCt of cells cultured with and without sulfide respectively. The primers are listed in Table S10.
D. Time course of sulfide concentration during sulfide oxidation activity using whole-cell of IM2438^T. The orange, blue and green lines represent the cells cultured with sulfide (Sul), without sulfide (CK) and with sulfide but heat-killed (Sul-Boiling) respectively. The detailed parameters have been described in Experimental procedures. The data (C, D) are the mean values and standard deviations from three duplicates of parallel incubations.

proton-based energetics similar as the other aerobic or facultatively aerobic alkaliphiles (Hicks *et al*., 2010).

Interestingly, we found that SQR may function in the stimulation of cell growth by sulfide (Figs 6 and 7). Oxidation of inorganic sulfur supplies reducing power or energy for chemolithotrophs and purple sulfur bacteria (Sorokin and Kuenen, 2005; Grimm *et al*., 2008; Berben *et al*., 2019). Reduced inorganic sulfur compounds have been reported to be oxidized by other obligate organotrophic bacteria (Sorokin, 2003; Hou *et al*., 2018). SQR is used for sulfide detoxification by heterotrophs, while transferring electrons to quinone and producing

quinol (Marcia *et al*., 2010). Subsequently, quinol can be oxidized via the electron respiratory chain (complexes III, IV and V) under aerobic or microaerobic conditions and a transmembrane proton gradient may form for ATP regeneration. In fact, sulfide could simultaneously decrease the oxygen concentration as a reductant. However, the culture conditions of both adding sulfide and reducing shaking speed could decrease oxygen concentration but lead to opposite effects on growth (Fig. 6D). Considering the upregulation of *sqr* at the transcriptional and enzymatic levels, we inferred that sulfide oxidation for ATP regeneration rather than a hypoxic environment was a reasonable explanation. This claim was supported by another hint that the extent of improvement in the growth rate under 75 rpm shaking was higher than that at 200 rpm (Fig. 6D), and the reason for this may be that more sulfide was oxidized biologically but not chemically under low oxygen concentration. SQR can detoxify sulfide and is also important for reducing sulfide toxicity. In addition, the ionic form of sulfide (HS^-) under alkaline conditions has been found to exhibit much lower toxicity than the non-ionized form under neutral pH (Sorokin *et al*., 2015); therefore, the finding that sulfide accelerates the cell growth and improves the adaptability in saline and alkaline environments may also exist in other heterotrophic microbes.

Spiribacter halalkaliphilus could utilize light and inorganic sulfide but depend on the organic compounds as main energy and carbon sources. Considering that there is no growth under anaerobic conditions, even with a light, oxidative phosphorylation is still the main pathway of energy generation. It is completely different from photoheterotrophs, which use light as the sole or main energy source and depend on organic carbon as the sole carbon source, for example, photoheterotrophy in *Heliobacterium chlorum* (Gest and Favinger, 1983) and *Rhodobacter capsulatus* (Gregor and Klug, 1999; Sawicki and Willows, 2007). In addition, in the presence of sulfide, both organic and inorganic compounds may fuel IM2438^T, and this trophic type belongs to litho-heterotrophy (Sorokin, 2003); however, a direct energetic evidence has yet to be provided.

Spiribacter halalkaliphilus was able to degrade several simple organic acids (lactate, pyruvate and acetate) and transform them into insoluble organic carbon (e.g. PHB) for carbon storage (Fig. 3E). The accumulation of intracellular PHB may improve microbial survival and stress tolerance in changing environments (López *et al*., 1995). This process changes the form of carbon in natural environments and impacts microbial community composition (Pinnell and Turner, 2019). In addition, there is usually sufficient sunlight in the brine of soda lakes (Grant and Sorokin, 2011). Multiple dissimilatory sulfur reduction pathways to supply sulfide in soda lakes, including the reduction of sulfate, sulfite, thiosulfate, elemental sulfur and polysulfide, have also been detected using metatranscriptomic studies (Edwardson and Hollibaugh, 2017; Vavourakis *et al*., 2019), and vast numbers of culturable sulfur-reducing bacteria and archaea been obtained (Sorokin *et al*., 2014; Sorokin *et al*., 2018). *S. halalkaliphilus* was able to utilize light energy and oxidize sulfide (Figs 5, 6 and 7), and metatranscriptomic research revealed that this abundant bacterium may participate in light energy conversion and the sulfur cycle (Fig. 4). Light and reductive sulfur compounds can provide energy for ATP synthesis and have been reported to stimulate carbon assimilation by heterotrophs (Tuttle and Jannasch, 1977; Palovaara *et al*., 2014). Similarly, anaplerotic carbon dioxide assimilation may also occur in *S. halalkaliphilus*.

The species *S. halalkaliphilus* was identified as the most abundant taxon in some ponds of soda-saline lakes, which could be considered open microbial habitats, such as neutral salterns (Oren and Hallsworth, 2014). Given the excellent adaptability to double extremes and metabolic capability of sulfide oxidation and PHB accumulation, it may be applied in biodesulfurization and bioplastic production with less contamination by other microorganisms.

Taken together, culture-dependent experiments and culture-independent metatranscriptomic procedures in this study have provided comprehensive insights into the physiological features, multiple environmental adaptation strategies, and ecological functions of the abundant microbes in saline and alkaline environments. Similarly, this research strategy could be employed for most other microbial taxa, as well as other habitats.

Description of Spiribacter halalkaliphilus *sp. nov.*

Spiribacter halalkaliphilus (Hal. al. ka. li'phi.lus. Gr. masc. n. *hals halos* salt; N.L. n. *alkali* alkali; Gr. masc. adj. *philus* friend, loving; N.L. masc. adj. *halalkaliphilus* salt and alkali-loving).

The cells are curved rods or short spirals. The cells are 0.2–0.3 μm wide and 0.5–1.5 μm long. Colonies are light purple, smooth, convex, round and 1.0–2.0 mm in diameter when cultured on the SH10 plate at 37°C for 3–5 days. Growth occurs in the presence of 3%–27% (wt./vol.) total salinity (optimum 10%–11%) at pH 8.0–11.0 (optimum pH 9.0). It is highly abundant (up to 15.63%) in soda-saline brines with a salinity of 15%–22%. Anaerobic growth did not occur in the presence of nitrate, L-arginine, or DMSO. The following substrates are utilized as single carbon and energy sources for growth: lactate, pyruvate and acetate. The following substrates are not utilized as

sole sources of carbon and energy: arabinose, cellobiose, ethanol, fructose, galactose, glucose, glycerol, lactose, maltose, raffinose, rhamnose, ribose, salicin, sorbose, starch, trehalose, alanine, arginine, aspartate, cysteine, glycine, glutamate, histidine, isoleucine, lysine, methionine, serine, valine, citrate, formate, gluconate, malate, malonate and succinate. The bacterial cells accumulate PHB granules, and the bacterium cell growth is stimulated by light (under microaerobic conditions) and sulfide.

The type strain, IM2438^T (=CGMCC 1.19110^T), was isolated from the sediment of Hutong Qagan Lake in Erdos, Inner Mongolia Autonomous Region, China. The genomic DNA G + C content of this strain is 64.2 mol.% (determined from the genome sequence). The GenBank accession number of the 16S rRNA gene sequence of strain IM2438^T is MN713357. The GenBank accession number of the genome sequence of strain IM2438^T is CP046046.

Experimental procedures

Sample source and physiochemical characterization for isolation

Brine (or water) and sediment samples from the following alkaline hypersaline inland lakes were used: Azzan-Nur, Bayan-Nur, Dalaru, Habor, Hutong Qagan, Sobenoor, Qagan and Yanhaizi lakes. All these lakes are located in the southwest of the Inner Mongolia Autonomous Region of China. The brine samples were collected in sterilized bottles, while that for the surface and deep sediment samples in sealed bags in 2017–2018. These samples were transported to the laboratory at ambient temperature of approximately 5–20°C in April 2017 and 20–30°C in July 2017 and August 2018, and then stored in a refrigerated room at 4–8°C. The locations of the ponds, together with the physicochemical parameters determined using previously described methods (Zhao *et al*., 2020), are listed in Table S1. Eighteen shared samples used for metagenomic sequencing were also used for microbial isolation and are marked in red.

Isolation of haloalkaliphiles and comparison with MAGs

Some previously reported neutral and alkaline media (Sehgal and Gibbons, 1960; Ventosa *et al*., 1982; Tindall *et al*., 1984; Gorlenko *et al*., 2009; Mou *et al*., 2012) were used in this study. To simulate natural environments, we prepared a series of PSM with inorganic compositions similar to those of soda-saline lakes. To isolate microorganisms with specific metabolic capability, alternative carbons (e.g. organic acids and methanol) or sulfur sources (e.g. sulfide, thiosulfate) were used in LN, LH, ME and SB series media. The pH was adjusted using HCl or NaOH solution. A solid medium was prepared by adding agar at a final concentration of 1.5% (wt./wt.). The agar was autoclaved separately in an alkaline medium. Detailed information about the composition of the media is provided in Table S2.

The brine or sediment samples were diluted to two gradients of 10^{-1} and 10^{-3} using similar NaCl concentrations, and 100 μl of diluent was spread on the surfaces of various agar plates, which were then incubated at 37°C referring to Halohandbook (Dyall-Smith, 2009) or a lower temperature of 28°C (Lagier *et al*., 2015). Generally, the culture time ranged from 1 to 30 days until colonies formed, and then they were selected and transferred to identical agar plates. The selection of colonies was based on morphological observations, such as shape, size, colour and wrinkles. The microorganisms were preserved at 3–5 copies at −80°C in a 20% (vol./vol.) glycerol solution with NaCl, and the salinity of glycerol stocks corresponded with the isolation media for different isolates.

For PCR, genomic DNA of the bacterial/archaeal colonies or lawn was extracted using a phenol-chloroform extraction (phenol:chloroform, 1:1 by volume). Briefly, bacterial/archaeal cells were added to the mixture of 450 μl double distilled water and 50 μl phenol-chloroform (pH 8.0). After rapid vortex and centrifugation, the aqueous phase was used as template for PCR. The 16S rRNA gene was amplified using PCR, and the primers used were 27F (5′-AGAGTTTGATCCTGGCTCAG-3′) and 1492R (5′-GGTTACCTTGTTACGACTT-3′) for bacteria (Frank *et al*., 2008) and 0018F (5′-ATTCCGGTTGATCC TGCC-3′) and 1518R (5′-AGGAGGTGATCCAGCCGC-3′) for archaea (Cui *et al*., 2009). PCR was performed with Taq DNA polymerase in a thermal cycler (Eppendorf, Hamburg, Germany) for 30 cycles according to the standard protocol. The PCR product was examined on a 1% (wt./vol.) agarose gel and sequenced by a commercial company (Witon Information Technology, Beijing, China). Subsequently, the 16S rRNA genes were used as queries to search the EzBioCloud to identify the taxonomic status (Yoon *et al*., 2017).

The similarity of the 16S rRNA gene between the isolates and 385 dereplicated MAGs from soda-saline lakes (Zhao *et al*., 2020) was analysed using local Nucleotide-Nucleotide BLAST 2.6.0+. In summary, 335 sequences of the 16S rRNA gene were retrieved from 909 original MAGs in this study, and they represented 168 of 385 dereplicated MAGs. The 18 metagenomes and coverage of 385 MAGs are described in a previous study (Zhao *et al*., 2020). To quantify the read percentage in metagenomes, the reads were mapped against the whole genome of IM2438^T using HISAT2 with default parameters (Kim *et al*., 2015), and paired and total reads were

counted using Samtools (Danecek *et al*., 2021). For the phylogenetic analysis of the 16S rRNA genes, multiple sequence alignment of the nucleotide was performed using the ClustalW program (Thompson *et al*., 1994). After trimming the poorly aligned ends, the phylogenetic trees were reconstructed using the maximum-likelihood algorithm integrated into MEGA 7 (Felsenstein, 1981; Kumar *et al*., 2008).

Genomic sequencing and analysis

Genomic DNA was extracted and purified for genomic sequencing using Qiagen DNA extraction kit of Blood & Cell Culture DNA Midi Kit (Catalogue No. 13343; QIAGEN, Dusseldorf, Germany) according to the manufacturer's instructions. Genomic DNA was sequenced using a combined Illumina HiSeq and Nanopore sequencing approach (Nextomics Biosciences). Genome assembly was performed using Canu version 1.7.11 with default parameters (Koren *et al*., 2017), followed by error correction using Pilon version 1.22 (Walker *et al*., 2014). The whole-genome sequence was annotated using the NCBI Prokaryotic Genome Annotation Pipeline. This genome has been included in the KEGG Genome database (Entry: T06294), and the metabolic pathway was reconstructed by referring the KEGG pathway maps. The Na+-translocating NADH: ubiquinone oxidoreductase (Na^+-NQR) is not included in the KEGG Orthology database, and COG1726, COG1805, COG2869, COG1347, COG2209, COG2871 and COG8991 were manually checked for its seven subunits. A total of 120 ubiquitous single-copy proteins were retrieved and concatenated using GTDB-Tk with default parameters (Parks *et al*., 2018; Chaumeil *et al*., 2020), and the maximum-likelihood tree was reconstructed using MEGA 7 software (Kumar *et al*., 2008). The genome-based relatedness between strain IM2438^T and closely related genomes or MAGs of the genus *Spiribacter* was determined based on the ANI (Richter and Rosselló-Móra, 2009) using the JSpeciesWS web server (http://jspecies.ribohost.com/jspeciesws/#analyse) for both ANIb (ANI with BLAST) and ANIm (ANI with Mummer), and *in silico* DNA–DNA hybridization was calculated using the genome-to-genome distance calculator (https://ggdc.dsmz.de/ggdc.php) (Meier-Kolthoff *et al*., 2013). Genome-level overall similarity was calculated, and heatmap visualization was performed using OrthoANI (Lee *et al*., 2016). The contigs of the GPB-6 draft genome were reordered according to the complete genome of strain IM2438^T using Mauve (Darling *et al*., 2011). The isoelectric points for proteomes were estimated using the Isoelectric Point Calculator (Kozlowski, 2016). The signal peptide sequence and transmembrane region were predicted using the online SignalP-5.0 Server (http://www.cbs.dtu.dk/services/SignalP/) and TMHMM Server v. 2.0 (http://www.cbs.dtu.dk/services/TMHMM/) respectively. For the phylogenetic analyses of xanthorhodopsin and SQR, the multiple sequence alignments of the amino acid sequences were performed using the ClustalW that is integrated in MEGA 7 with default parameters (Thompson *et al*., 1994), and the maximum likelihood trees were reconstructed using the MEGA 7 (Felsenstein, 1981; Kumar *et al*., 2008).

Physiological characterization of IM2438^T

The ingredients of the optimal medium (named SH10) for *S. halalkaliphilus* are as follows (per litre): NaCl, 50 g; $NaHCO_3$, 20 g; Na_2CO_3, 20 g; $MgSO_4$, 1 g; Na_2SO_4, 12 g; KH_2PO_4, 0.06 g; KCl, 2 g; $CaCl_2$, 2 g; yeast extract, 0.25 g; KNO_3, 0.3 g; trace element solution SL-6, 1 ml; $FeSO_4$, 2.5 mg; vitamin 10 stock solution, 3 ml; and lactate, 5 g. The compositions of SL-6 and vitamin 10 stock solutions are described in the Halohandbook (Dyall-Smith, 2009). The pH was approximately 9.0. The total salinity was approximately 10% in SH10, while NaCl increased up to 150 g L^{-1} in SH20 to exert higher salinity stress. Liquid medium was used in the routine culture at 37°C with shaking at 200 rpm. Cell growth was determined by measuring the optical density at 600 nm using a UV/Vis spectrophotometer (Yoke Instrument, China). The solid medium was prepared by adding autoclaved agar separately at a final concentration of 1.5% (wt./wt.). Cell numbers were quantified using the plate count method; 200 μl of serial diluent was loaded on solid medium, and then incubated at 37°C for approximately 7 days. Diluents from which approximately 50–500 colonies formed on the surface of solid media were used to calculate the CFUs. Cell morphology was observed using scanning electron microscopy (SEM), as previously described (Hou *et al*., 2015). Briefly, the cells were fixed with 2.5% glutaraldehyde in phosphate-buffered saline containing 10% NaCl, dehydrated, and subjected to gold plating before observation using an SEM FEI Quanta 200. PHB granules were observed using TEM (Cai *et al*., 2012). In brief, after fixation with 1.0% osmium tetroxide overnight, TEM analysis was performed according to the standard protocol. Micrographs were recorded using a Tecnai 20 electron microscope (Thermo Fisher Scientific, Waltham, MA, USA).

The range of salinity for growth was set from 0% to 30% at intervals of 1% (wt./vol.) at pH 9.0. When the total salinity was 5%–30%, the predominant inorganic salts had varying concentrations of NaCl, 20 g L^{-1} Na_2CO_3, 20 g L^{-1} $NaHCO_3$ and 12 g L^{-1} Na_2SO_4; and the buffer system was Na_2CO_3/$NaHCO_3$. When the total salinity

was 0%–5%, the predominant inorganic salt was NaCl at varying concentrations (no Na_2CO_3, $NaHCO_3$, or Na_2SO_4), and the buffer system was 25 mM CHES. The pH range for growth was adjusted from pH 7.0–12.0 at intervals of 0.5 units with 100 g L^{-1} NaCl. The buffer systems were HEPES (pH 6.8–8.0), Tricine (pH 7.4–8.8), CHES (pH 8.6–10.0) and CAPS (pH 9.7–12.0), all at 25 mM. Anaerobic growth was performed in SH10 medium by static cultivation in screw-capped bottles with nitrogen, while microaerobic growth was performed by static cultivation in screw-capped bottles with air, or cultivation in flasks with shaking at 75 and 40 rpm. Anaerobic respiration was tested by adding 5 g L^{-1} potassium nitrate (50 mM), L-arginine (29 mM), or 5 ml L^{-1} DMSO (71 mM). To test the utilization of sole carbon and energy sources, yeast extract was reduced to 0.1 g L^{-1} in SH10 medium, and the different substrates were added individually at a concentration of 5 g L^{-1}. A total of 37 types of carbon sources were used, namely, arabinose (33 mM), cellobiose (15 mM), ethanol (109 mM), fructose (28 mM), galactose (28 mM), glucose (28 mM), glycerol (54 mM), lactose (17 mM), maltose (15 mM), raffinose (10 mM), rhamnose (30 mM), ribose (33 mM), salicin (17 mM), sorbose (28 mM), starch, trehalose (13 mM), alanine (56 mM), arginine (29 mM), aspartate (38 mM), cysteine (41 mM), glycine (67 mM), glutamate (30 mM), histidine (32 mM), isoleucine (38 mM), lysine (34 mM), methionine (34 mM), serine (48 mM), valine (43 mM), acetate (83 mM), citrate (26 mM), formate (48 mM), gluconate (26 mM), lactate (56 mM) (same as in SH10), malate (37 mM), malonate (48 mM), pyruvate (45 mM) and succinate (43 mM). To explore the effect of light on cell growth, the carbon source concentration was decreased to 0.5 g L^{-1}. An illumination incubator ZQLY-180GF (Shanghai Zhichu Instrument, Shanghai, China) with a light intensity of 6000 Lux by LED was used to estimate the effect of light. Fifteen millimolarity sodium sulfide was added to estimate its effect, and the concentration was based on a previous report (Spring *et al*., 2001).

The residual lactate in the supernatant was determined using a biosensor analyser SBA-40C (Biology Institute of Shandong Academy of Sciences, Jinan, China), which could be used for saline and alkaline samples. Bacteria were harvested via centrifugation at 10 000*g* for 10 min and then washed once with 10% NaCl solution. CDW was measured by weighing after lyophilization, and the PHB mass was detected using gas chromatography (Lu *et al*., 2008b). Briefly, lyophilized cells were subjected to methanolysis in a mixture of chloroform and methanol containing 3% (vol./vol.) sulfuric acid at 100°C for 4 h, and then hydroxyacyl methylesters were analysed with Agilent GC-6820. Benzoic acid was used as an internal standard for the quantitative analysis. All tests were performed in duplicates with parallel incubations.

RNA extraction and qRT-PCR

The strain was grown in SH10 medium with or without sulfide until the exponential phase with an OD_{600} of 0.35–0.40. The cells were harvested for total RNA extraction using TRIzol reagent (Invitrogen, USA) as previously described (Lu *et al*., 2008a). DNA was removed from total RNA using a TURBO DNA-free™ Kit (Thermo Fisher Scientific) and was checked using PCR. DNA-free RNA (1 μg) was used to synthesize cDNA using random hexamers and murine leukaemia virus reverse transcription (Promega Corporation, Fitchburg, WI, USA). The relative fold change in gene expression was analysed using a ViiA 7 real-time PCR system (Applied Biosystems, Foster City, CA, USA) and 16S rRNA as an endogenous control to normalize the data of each sample. The fold change was calculated using the Delta–Delta Ct method and the formula $2^{\wedge}[-((Ct_{interest} - Ct_{16S})_{Sul} - (Ct_{interest} - Ct_{16S})_{CK})]$, where $Ct_{interest}$ and Ct_{16S} indicate the Ct values of the cDNA of interest and 16S rRNA, while Sul and CK are the ΔCt values of cells cultured with and without sulfide respectively. The Ct values of three replicates were averaged for one sample, and duplicates of parallel incubations were performed. The primers used for qRT-PCR are listed in Table S10.

Sulfide oxidation activity

The method for determining whole-cell sulfide oxidation enzyme activity was modified from a previous study (Hou *et al*., 2018). In brief, the cells were grown in SH10 medium with or without sulfide to an OD_{600} of approximately 0.2, harvested by centrifugation (6000 rpm for 5 min), and suspended in 50 mM Tris–HCl buffer containing 10% NaCl (pH 8.0–8.1). For the heat-killed control, the suspended cells were incubated in boiling water for 10 min and cooled to room temperature (approximately 20–25°C). The cell suspension was transferred into a 15 ml capping tube, and approximately 1 mM freshly prepared Na_2S was added to initiate the biochemical reaction. The tube was incubated at 30°C with shaking at 100 rpm. The concentration of the residual sulfide was determined using a commercial hydrogen sulfide (H_2S) assay kit (Jiancheng Company, Nanjing, China) according to the manufacturer's instructions. The experiment was performed in duplicates with parallel incubations.

Metatranscriptomic experiment and bioinformatics analysis

The microbial cells were collected from brine samples of approximately 1–5 L by 0.8- and 0.22-μm size filters and

then stored in plastic tubes in liquid nitrogen. The samples were transported to the laboratory on dry ice. The filters were used to extract total RNA with an RNeasy PowerSoil Total RNA kit (QIAGEN, Hilden, Germany), and DNA contamination was removed using DNase (Takara Bio, Shiga, Japan). After quantification and quality checking, ribosomal RNA was removed by using a Ribo-Zero rRNA removal kit (Illumina, USA), and then the enriched mRNA was used to construct a library for strand-specific metatranscriptomic sequencing. The sequencing was performed on a NovaSeq platform (Illumina, San Diego, CA, USA) by a commercial company (Magigene, Guangzhou, China). Clean data were obtained using the raw read QC module (read_qc) with default parameters in MetaWRAP (Uritskiy *et al*., 2018). The clean reads, clean bases, error rate, Q20, Q30 and GC content of the clean data are summarized in Table S7. The reads were mapped against the whole genome of *S. halalkaliphilus* using HISAT2 with default parameters (Kim *et al*., 2015), and the number of reads mapped to the reverse-stranded cDNA of each gene was counted using featureCount (Liao *et al*., 2014). The data on read numbers were saved in DATA SET 1. The coverage was estimated using Samtools (Danecek *et al*., 2021). The TPM value of each gene in each sample was calculated using the equation ($TPM_i = N_i/L_i \times 10^6/\sum_{k=1}^{n} N_k/L_k$, in which TPM_i, N_i and L_i are the TPM value, read number and gene length of gene *i* respectively; n is the number of total genes in the *S. halalkaliphilus* genome). Transcription activity was expressed as TPM and qualitatively grouped by the percentage ratio of TPM to the average transcripts per million: very high, >500%; high, 200%–500%; normal, 20%–200%; and low/not, <20%.

Acknowledgements

This study was supported by the National Natural Science Foundation of China (No. 91751201), the National Key R&D Program of China (No. 2020YFA0906800) and the Science and Technology Basic Resources Investigation Project (No. 2017FY100300). We would like to thank the reviewers for their constructive comments to help us improve the manuscript.

Author Contributions

Q.X., D.Z. and H.X. conceived the work. Q.X. isolated the strains and carried out most experiments. D.Z. performed the most bioinformatic analysis and designed most experiments. S.Z. performed the analysis of alignment between isolates and MAGs. S.Z. and H.Z. prepared the samples for metatranscriptomic sequencing. Z.Z. participated in the physiological identification. J.Z. participated in the sample collection and strain isolation. M.L. participated in the data analysis. Q.X. and D.Z. prepared the results and wrote the manuscript under the guidance of H.X. All authors read and approved the final manuscript.

Data Availability Statement

The 16S rRNA gene sequences of the cultured isolates have been deposited in the GenBank, and the accession numbers are listed in Table S3. The accession number of the *S. halalkaliphilus* IM2438^T genome is CP046046. The raw reads of the metatranscriptomic sequencing have been deposited in the NCBI as BioProject PRJNA645844.

References

Asao, M., Pinkart, H.C., and Madigan, M.T. (2011) Diversity of extremophilic purple phototrophic bacteria in soap Lake, a Central Washington (USA) soda lake. *Environ Microbiol* **13**: 2146–2157. https://doi.org/10.1111/j.1462-2920.2011.02449.x.

Banciu, H.L., and Muntyan, M.S. (2015) Adaptive strategies in the double-extremophilic prokaryotes inhabiting soda lakes. *Curr Opin Microbiol* **25**: 73–79. https://doi.org/10.1016/j.mib.2015.05.003.

Berben, T., Overmars, L., Sorokin, D.Y., and Muyzer, G. (2019) Diversity and distribution of sulfur oxidation-related genes in *Thioalkalivibrio*, a genus of chemolithoautotrophic and haloalkaliphilic sulfur-oxidizing bacteria. *Front Microbiol* **10**: 160. https://doi.org/10.3389/Fmicb.2019.00160.

Boros, E., and Kolpakova, M. (2018) A review of the defining chemical properties of soda lakes and pans: an assessment on a large geographic scale of Eurasian inland saline surface waters. *PLoS One* **13**: e0202205. https://doi.org/10.1371/journal.pone.0202205.

Cai, S.F., Cai, L., Liu, H.L., Liu, X.Q., Han, J., Zhou, J., *et al*. (2012) Identification of the haloarchaeal phasin (PhaP) that functions in polyhydroxyalkanoate accumulation and granule formation in *Haloferax mediterranei*. *Appl Environ Microbiol* **78**: 1946–1952. https://doi.org/10.1128/Aem.07114-11.

Chaumeil, P.A., Mussig, A.J., Hugenholtz, P., and Parks, D. H. (2020) GTDB-Tk: a toolkit to classify genomes with the genome taxonomy database. *Bioinformatics* **36**: 1925–1927. https://doi.org/10.1093/bioinformatics/btz848.

Cui, H.L., Zhou, P.J., Oren, A., and Liu, S.J. (2009) Intraspecific polymorphism of 16S rRNA genes in two halophilic archaeal genera, *Haloarcula* and *Halomicrobium*. *Extremophiles* **13**: 31–37. https://doi.org/10.1007/s00792-008-0194-2.

Danecek, P., Bonfield, J.K., Liddle, J., Marshall, J., Ohan, V., Pollard, M.O., *et al*. (2021) Twelve years of SAMtools and BCFtools. *GigaScience* **10**: giab008. https://doi.org/10.1093/gigascience/giab008.

Darling, A.E., Tritt, A., Eisen, J.A., and Facciotti, M.T. (2011) Mauve assembly metrics. *Bioinformatics* **27**: 2756–2757. https://doi.org/10.1093/bioinformatics/btr451.

Dyall-Smith M. (2009) *Halohandbook*. URL https://haloarchaea.com/halohandbook/.

Edwardson, C.F., and Hollibaugh, J.T. (2017) Metatranscriptomic analysis of prokaryotic communities active in sulfur and arsenic cycling in Mono Lake, California, USA. *ISME J* **11**: 2195–2208. https://doi.org/10.1038/ismej.2017.80.

Felsenstein, J. (1981) Evolutionary trees from DNA-sequences – a maximum-likelihood approach. *J Mol Evol* **17**: 368–376. https://doi.org/10.1007/Bf01734359.

Frank, J.A., Reich, C.I., Sharma, S., Weisbaum, J.S., Wilson, B.A., and Olsen, G.J. (2008) Critical evaluation of two primers commonly used for amplification of bacterial 16S rRNA genes. *Appl Environ Microbiol* **74**: 2461–2470. https://doi.org/10.1128/Aem.02272-07.

Gest, H., and Favinger, J.L. (1983) *Heliobacterium chlorum*, an anoxygenic brownish-green photosynthetic bacterium containing a "new" form of bacteriochlorophyll. *Arch Microbiol* **136**: 11–16. https://doi.org/10.1007/Bf00415602.

Giovannoni, S.J. (2017) SAR11 bacteria: the most abundant plankton in the oceans. *Ann Rev Mar Sci* **9**: 231–255. https://doi.org/10.1146/annurev-marine-010814-015934.

Giovannoni, S.J., Tripp, H.J., Givan, S., Podar, M., Vergin, K.L., Baptista, D., *et al*. (2005) Genome streamlining in a cosmopolitan oceanic bacterium. *Science* **309**: 1242–1245. https://doi.org/10.1126/science.1114057.

Gorlenko, V.M., Bryantseva, I.A., Rabold, S., Tourova, T.P., Rubtsova, D., Smirnova, E., *et al*. (2009) *Ectothiorhodospira variabilis* sp. nov., an alkaliphilic and halophilic purple sulfur bacterium from soda lakes. *Int J Syst Evol Microbiol* **59**: 658–664. https://doi.org/10.1099/ijs.0.004648-0.

Grant, W.D., and Sorokin, D.Y. (2011) Distribution and diversity of soda lake alkaliphiles. In *Extremophiles Handbook*, Horikoshi, K. (ed). Tokyo: Springer Japan, pp. 27–54. https://doi.org/10.1007/978-4-431-53898-1_3.

Gregor, J., and Klug, G. (1999) Regulation of bacterial photosynthesis genes by oxygen and light. *FEMS Microbiol Lett* **179**: 1–9.

Grimm, F., Franz, B., and Dahl, C. (2008) Thiosulfate and sulfur oxidation in purple sulfur bacteria. In *Microbial Sulfur Metabolism*, Dahl, C., and Friedrich, C.G. (eds). Berlin, Heidelberg: Springer. https://doi.org/10.1007/978-3-540-72682-1_9.

Gunde-Cimerman, N., Plemenitaš, A., and Oren, A. (2018) Strategies of adaptation of microorganisms of the three domains of life to high salt concentrations. *FEMS Microbiol Rev* **42**: 353–375. https://doi.org/10.1093/femsre/fuy009.

Hicks, D.B., Liu, J., Fujisawa, M., and Krulwich, T.A. (2010) F_1F_0-ATP synthases of alkaliphilic bacteria: lessons from their adaptations. *Biochim Biophys Acta-Bioenerg* **1797**: 1362–1377. https://doi.org/10.1016/j.bbabio.2010.02.028.

Hoeft, S.E., Blum, J.S., Stolz, J.F., Tabita, F.R., Witte, B., King, G.M., *et al*. (2007) *Alkalilimnicola ehrlichii* sp. nov., a novel, arsenite-oxidizing haloalkaliphilic gammaproteobacterium capable of chemoautotrophic or heterotrophic growth with nitrate or oxygen as the electron acceptor. *Int J Syst Evol Microbiol* **57**: 504–512. https://doi.org/10.1099/ijs.0.64576-0.

Hou, J., Xiang, H., and Han, J. (2015) Propionyl coenzyme A (Propionyl-CoA) carboxylase in *Haloferax mediterranei*: indispensability for propionyl-CoA assimilation and impacts on global metabolism. *Appl Environ Microbiol* **81**: 794–804. https://doi.org/10.1128/Aem.03167-14.

Hou, N.K., Xia, Y.Z., Wang, X., Liu, H.W., Liu, H.L., and Xun, L.Y. (2018) H_2S biotreatment with sulfide-oxidizing heterotrophic bacteria. *Biodegradation* **29**: 511–524. https://doi.org/10.1007/s10532-018-9849-6.

Ito, M., Guffanti, A.A., Oudega, B., and Krulwich, T.A. (1999) *mrp*, a multigene, multifunctional locus in *Bacillus subtilis* with roles in resistance to cholate and to Na^+ and in pH homeostasis. *J Bacteriol* **181**: 2394–2402.

Jain, C., Rodriguez-R, L.M., Phillippy, A.M., Konstantinidis, K.T., and Aluru, S. (2018) High throughput ANI analysis of 90K prokaryotic genomes reveals clear species boundaries. *Nat Commun* **9**: 5114. https://doi.org/10.1038/s41467-018-07641-9.

Kaim, G., Wehrle, F., Gerike, U., and Dimroth, P. (1997) Molecular basis for the coupling ion selectivity of F_1F_0 ATP synthases: probing the liganding groups for Na^+ and Li^+ in the *c* subunit of the ATP synthase from *Propionigenium modestum*. *Biochemistry-Us* **36**: 9185–9194. https://doi.org/10.1021/bi970831q.

Kim, D., Langmead, B., and Salzberg, S.L. (2015) HISAT: a fast spliced aligner with low memory requirements. *Nat Methods* **12**: 357–360. https://doi.org/10.1038/nmeth.3317.

Kim, M., Oh, H.S., Park, S.C., and Chun, J. (2014) Towards a taxonomic coherence between average nucleotide identity and 16S rRNA gene sequence similarity for species demarcation of prokaryotes. *Int J Syst Evol Microbiol* **64**: 346–351. https://doi.org/10.1099/ijs.0.059774-0.

Koren, S., Walenz, B.P., Berlin, K., Miller, J.R., Bergman, N.H., and Phillippy, A.M. (2017) Canu: scalable and accurate long-read assembly via adaptive k-mer weighting and repeat separation. *Genome Res* **27**: 722–736. https://doi.org/10.1101/gr.215087.116.

Kozlowski, L.P. (2016) IPC – Isoelectric Point Calculator. *Biol Direct* **11**: 55. https://doi.org/10.1186/s13062-016-0159-9.

Krulwich, T.A., Sachs, G., and Padan, E. (2011) Molecular aspects of bacterial pH sensing and homeostasis. *Nat Rev Microbiol* **9**: 330–343. https://doi.org/10.1038/nrmicro2549.

Kumar, S., Nei, M., Dudley, J., and Tamura, K. (2008) MEGA: a biologist-centric software for evolutionary analysis of DNA and protein sequences. *Brief Bioinform* **9**: 299–306. https://doi.org/10.1093/bib/bbn017.

Lagier, J.C., Edouard, S., Pagnier, I., Mediannikov, O., Drancourt, M., and Raoult, D. (2015) Current and past strategies for bacterial culture in clinical microbiology. *Clin Microbiol Rev* **28**: 208–236. https://doi.org/10.1128/Cmr.00110-14.

Lanzén, A., Simachew, A., Gessesse, A., Chmolowska, D., Jonassen, I., and Øvreås, L. (2013) Surprising prokaryotic and eukaryotic diversity, community structure and

biogeography of Ethiopian soda lakes. *PLoS One* **8**: e72577. https://doi.org/10.1371/journal.pone.0072577.

Lee, I., Ouk, K.Y., Park, S.C., and Chun, J. (2016) OrthoANI: an improved algorithm and software for calculating average nucleotide identity. *Int J Syst Evol Microbiol* **66**: 1100–1103. https://doi.org/10.1099/ijsem.0.000760.

Liao, Y., Smyth, G.K., and Shi, W. (2014) featureCounts: an efficient general purpose program for assigning sequence reads to genomic features. *Bioinformatics* **30**: 923–930. https://doi.org/10.1093/bioinformatics/btt656.

López, N.I., Floccari, M.E., Steinbüchel, A., García, A.F., and Méndez, B.S. (1995) Effect of poly(3-hydroxybutyrate) (PHB) content on the starvation-survival of bacteria in natural-waters. *FEMS Microbiol Ecol* **16**: 95–101. https://doi.org/10.1016/0168-6496(94)00073-6.

López-Pérez, M., Ghai, R., Leon, M.J., Rodríguez-Olmos, Á., Copa-Patiño, J.L., Soliveri, J., *et al*. (2013) Genomes of "Spiribacter", a streamlined, successful halophilic bacterium. *BMC Genomics* **14**: 787. https://doi.org/10.1186/1471-2164-14-787.

Lu, Q.H., Han, J., Zhou, L.G., Coker, J.A., DasSarma, P., DasSarma, S., *et al*. (2008a) Dissection of the regulatory mechanism of a heat-shock responsive promoter in haloarchaea: a new paradigm for general transcription factor directed archaeal gene regulation. *Nucleic Acids Res* **36**: 3031–3042. https://doi.org/10.1093/nar/gkn152.

Lu, Q.H., Han, J., Zhou, L.G., Zhou, J., and Xiang, H. (2008b) Genetic and biochemical characterization of the poly(3-hydroxybutyrate-co-3-hydroxyvalerate) synthase in *Haloferax mediterranei*. *J Bacteriol* **190**: 4173–4180. https://doi.org/10.1128/Jb.00134-08.

Marcia, M., Ermler, U., Peng, G.H., and Michel, H. (2010) A new structure-based classification of sulfide:quinone oxidoreductases. *Proteins* **78**: 1073–1083. https://doi.org/10.1002/prot.22665.

Maresca, J.A., Miller, K.J., Keffer, J.L., Sabanayagam, C.R., and Campbell, B.J. (2018) Distribution and diversity of rhodopsin-producing microbes in the Chesapeake Bay. *Appl Environ Microbiol* **84**: e00137-00118. https://doi.org/10.1128/AEM.00137-18.

Meier, T., Polzer, P., Diederichs, K., Welte, W., and Dimroth, P. (2005) Structure of the rotor ring of F-type Na^+-ATPase from *Ilyobacter tartaricus*. *Science* **308**: 659–662. https://doi.org/10.1126/science.1111199.

Meier-Kolthoff, J.P., Auch, A.F., Klenk, H.P., and Göker, M. (2013) Genome sequence-based species delimitation with confidence intervals and improved distance functions. *BMC Bioinformatics* **14**: 60. https://doi.org/10.1186/1471-2105-14-60.

Mesbah, N.M., Cook, G.M., and Wiegel, J. (2009) The halophilic alkalithermophile *Natranaerobius thermophilus* adapts to multiple environmental extremes using a large repertoire of Na^+ (K^+)/H^+ antiporters. *Mol Microbiol* **74**: 270–281.

Mikhodyuk, O.S., Gerasimenko, L.M., Akimov, V.N., Ivanovskiĭ, R.N., and Zavarzin, G.A. (2008) Ecophysiology and polymorphism of the unicellular extremely natronophilic cyanobacterium *Euhalothece* sp. Z-M001 from Lake Magadi. *Microbiology* **77**: 717–725. https://doi.org/10.1134/S0026261708060106.

Mou, Y.Z., Qiu, X.X., Zhao, M.L., Cui, H.L., Oh, D., and Dyall-Smith, M.L. (2012) *Halohasta litorea* gen. nov. sp. nov., and *Halohasta litchfieldiae* sp. nov., isolated from the Daliang aquaculture farm, China and from deep Lake, Antarctica, respectively. *Extremophiles* **16**: 895–901. https://doi.org/10.1007/s00792-012-0485-5.

Oren, A., and Hallsworth, J.E. (2014) Microbial weeds in hypersaline habitats: the enigma of the weed-like *Haloferax mediterranei*. *FEMS Microbiol Lett* **359**: 134–142. https://doi.org/10.1111/1574-6968.12571.

Oren, A., Heldal, M., Norland, S., and Galinski, E.A. (2002) Intracellular ion and organic solute concentrations of the extremely halophilic bacterium *Salinibacter ruber*. *Extremophiles* **6**: 491–498. https://doi.org/10.1007/s00792-002-0286-3.

Palovaara, J., Akram, N., Baltar, F., Bunse, C., Forsberg, J., Pedrós-Alió, C., *et al*. (2014) Stimulation of growth by proteorhodopsin phototrophy involves regulation of central metabolic pathways in marine planktonic bacteria. *Proc Natl Acad Sci U S A* **111**: E3650–E3658. https://doi.org/10.1073/pnas.1402617111.

Papke, R.T., Douady, C.J., Doolittle, W.F., and Rodríguez-Valera, F. (2003) Diversity of bacteriorhodopsins in different hypersaline waters from a single Spanish saltern. *Environ Microbiol* **5**: 1039–1045. https://doi.org/10.1046/j.1462-2920.2003.00501.x.

Parks, D.H., Chuvochina, M., Waite, D.W., Rinke, C., Skarshewski, A., Chaumeil, P.A., *et al*. (2018) A standardized bacterial taxonomy based on genome phylogeny substantially revises the tree of life. *Nat Biotechnol* **36**: 996–1004. https://doi.org/10.1038/nbt.4229.

Pinnell, L.J., and Turner, J.W. (2019) Shotgun metagenomics reveals the benthic microbial community response to plastic and bioplastic in a coastal marine environment. *Front Microbiol* **10**: 1252. https://doi.org/10.3389/fmicb.2019.01252.

Richter, M., and Rosselló-Móra, R. (2009) Shifting the genomic gold standard for the prokaryotic species definition. *Proc Natl Acad Sci U S A* **106**: 19126–19131. https://doi.org/10.1073/pnas.0906412106.

Sawicki, A., and Willows, R.D. (2007) S-Adenosyl-L-methionine: magnesium-protoporphyrin IX O-methyltransferase from *Rhodobacter capsulatus*: mechanistic insights and stimulation with phospholipids. *Biochem J* **406**: 469–478. https://doi.org/10.1042/Bj20070284.

Sehgal, S.N., and Gibbons, N.E. (1960) Effect of some metal ions on the growth of *Halobacterium cutirubrum*. *Can J Microbiol* **6**: 165–169. https://doi.org/10.1139/m60-018.

Sorokin, D.Y. (2003) Oxidation of inorganic sulfur compounds by obligately organotrophic bacteria. *Microbiology* **72**: 641–653. https://doi.org/10.1023/B:Mici.0000008363.24128.E5.

Sorokin, D.Y., Banciu, H.L., and Muyzer, G. (2015) Functional microbiology of soda lakes. *Curr Opin Microbiol* **25**: 88–96. https://doi.org/10.1016/j.mib.2015.05.004.

Sorokin, D.Y., Berben, T., Melton, E.D., Overmars, L., Vavourakis, C.D., and Muyzer, G. (2014) Microbial diversity and biogeochemical cycling in soda lakes. *Extremophiles* **18**: 791–809. https://doi.org/10.1007/s00792-014-0670-9.

Sorokin, D.Y., Detkova, E.N., and Muyzer, G. (2011) Sulfur-dependent respiration under extremely haloalkaline conditions in soda lake 'acetogens' and the description of *Natroniella sulfidigena* sp. nov. *FEMS Microbiol Lett* **319**: 88–95. https://doi.org/10.1111/j.1574-6968.2011.02272.x.

Sorokin, D.Y., Elcheninov, A.G., Toshchakov, S.V., Bale, N. J., Damsté, J.S.S., Khijniak, T.V., *et al*. (2019) *Natrarchaeobius chitinivorans* gen. nov., sp. nov., and *Natrarchaeobius halalkaliphilus* sp. nov., alkaliphilic, chitin-utilizing haloarchaea from hypersaline alkaline lakes. *Syst Appl Microbiol* **42**: 309–318. https://doi.org/10.1016/j.syapm.2019.01.001.

Sorokin, D.Y., Kublanov, I.V., Gavrilov, S.N., Rojo, D., Roman, P., Golyshin, P.N., *et al*. (2016) Elemental sulfur and acetate can support life of a novel strictly anaerobic haloarchaeon. *ISME J* **10**: 240–252. https://doi.org/10.1038/ismej.2015.79.

Sorokin, D.Y., and Kuenen, J.G. (2005) Haloalkaliphilic sulfur-oxidizing bacteria in soda lakes. *FEMS Microbiol Rev* **29**: 685–702. https://doi.org/10.1016/j.femsre.2004.10.005.

Sorokin, D.Y., Lysenko, A.M., Mityushina, L.L., Tourova, T. P., Jones, B.E., Rainey, F.A., *et al*. (2001) *Thioalkalimicrobium aerophilum* gen. nov., sp. nov. and *Thioalkalimicrobium sibericum* sp. nov., and *Thioalkalivibrio versutus* gen. nov., sp. nov., *Thioalkalivibrio nitratis* sp. nov., novel and *Thioalkalivibrio denitrificancs* sp. nov., novel obligately alkaliphilic and obligately chemolithoautotrophic sulfur-oxidizing bacteria from soda lakes. *Int J Syst Evol Microbiol* **51**: 565–580. https://doi.org/10.1099/00207713-51-2-565.

Sorokin, D.Y., Makarova, K.S., Abbas, B., Ferrer, M., Golyshin, P.N., Galinski, E.A., *et al*. (2017) Discovery of extremely halophilic, methyl-reducing euryarchaea provides insights into the evolutionary origin of methanogenesis. *Nat Microbiol* **2**: 17081. https://doi.org/10.1038/nmicrobiol.2017.81.

Sorokin, D.Y., Messina, E., La Cono, V., Ferrero, M., Ciordia, S., Mena, M.C., *et al*. (2018) Sulfur respiration in a group of facultatively anaerobic natronoarchaea ubiquitous in hypersaline soda lakes. *Front Microbiol* **9**: 2359. https://doi.org/10.3389/Fmicb.2018.02359.

Sorokin, D.Y., Tourova, T.P., Henstra, A.M., Stams, A.J.M., Galinski, E.A., and Muyzer, G. (2008) Sulfidogenesis under extremely haloalkaline conditions by *Desulfonatronospira thiodismutans* gen. nov., sp. nov., and *Desulfonatronospira delicata* sp. nov: a novel lineage of *Deltaproteobacteria* from hypersaline soda lakes. *Microbiology-SGM* **154**: 1444–1453. https://doi.org/10.1099/mic.0.2007/015628-0.

Spring, S., Kämpfer, P., and Schleifer, K.H. (2001) *Limnobacter thiooxidans* gen. nov., sp nov., a novel thiosulfate-oxidizing bacterium isolated from freshwater lake sediment. *Int J Syst Evol Microbiol* **51**: 1463–1470. https://doi.org/10.1099/00207713-51-4-1463.

Swartz, T.H., Ikewada, S., Ishikawa, O., Ito, M., and Krulwich, T.A. (2005) The Mrp system: a giant among monovalent cation/proton antiporters? *Extremophiles* **9**: 345–354. https://doi.org/10.1007/s00792-005-0451-6.

Thompson, J.D., Higgins, D.G., and Gibson, T.J. (1994) CLUSTAL W: improving the sensitivity of progressive multiple sequence alignment through sequence weighting, position-specific gap penalties and weight matrix choice. *Nucleic Acids Res* **22**: 4673–4680. https://doi.org/10.1093/nar/22.22.4673.

Tindall, B.J., Ross, H.N.M., and Grant, W.D. (1984) *Natronobacterium* gen. nov. and *Natronococcus* gen. nov., two new genera of haloalkaliphilic archaebacteria. *Syst Appl Microbiol* **5**: 41–57.

Tuttle, J.H., and Jannasch, H.W. (1977) Thiosulfate stimulation of microbial dark assimilation of carbon dioxide in shallow marine waters. *Microb Ecol* **4**: 9–25. https://doi.org/10.1007/BF02010426.

Uritskiy, G.V., DiRuggiero, J., and Taylor, J. (2018) MetaWRAP-a flexible pipeline for genome-resolved metagenomic data analysis. *Microbiome* **6**: 158. https://doi.org/10.1186/s40168-018-0541-1.

Vavourakis, C.D., Andrei, A.S., Mehrshad, M., Ghai, R., Sorokin, D.Y., and Muyzer, G. (2018) A metagenomics roadmap to the uncultured genome diversity in hypersaline soda lake sediments. *Microbiome* **6**: 168. https://doi.org/10.1186/S40168-018-0548-7.

Vavourakis, C.D., Ghai, R., Rodriguez-Valera, F., Sorokin, D.Y., Tringe, S.G., Hugenholtz, P., *et al*. (2016) Metagenomic insights into the uncultured diversity and physiology of microbes in four hypersaline soda lake brines. *Front Microbiol* **7**: 211. https://doi.org/10.3389/Fmicb.2016.00211.

Vavourakis, C.D., Mehrshad, M., Balkema, C., van Hall, R., Andrei, A.S., Ghai, R., *et al*. (2019) Metagenomes and metatranscriptomes shed new light on the microbial-mediated sulfur cycle in a Siberian soda lake. *BMC Biol* **17**: 69. https://doi.org/10.1186/s12915-019-0688-7.

Ventosa, A., Quesada, E., Rodriguez-Valera, F., Ruiz-Berraquero, F., and Ramos-Cormenzana, A. (1982) Numerical taxonomy of moderately halophilic Gram-negative rods. *J Gen Microbiol* **128**: 1959–1968.

Walker, B.J., Abeel, T., Shea, T., Priest, M., Abouelliel, A., Sakthikumar, S., *et al*. (2014) Pilon: an integrated tool for comprehensive microbial variant detection and genome assembly improvement. *PLoS One* **9**: e112963. https://doi.org/10.1371/journal.pone.0112963.

Yoon, S.H., Ha, S.M., Kwon, S., Lim, J., Kim, Y., Seo, H., and Chun, J. (2017) Introducing EzBioCloud: a taxonomically united database of 16S rRNA gene sequences and whole-genome assemblies. *Int J Syst Evol Microbiol* **67**: 1613–1617. https://doi.org/10.1099/ijsem.0.001755.

Zhao, D., Zhang, S., Xue, Q., Chen, J., Zhou, J., Cheng, F., *et al*. (2020) Abundant taxa and favorable pathways in the microbiome of soda-saline lakes in Inner Mongolia. *Front Microbiol* **11**: 1740. https://doi.org/10.3389/fmicb.2020.01740.

Zorz, J.K., Sharp, C., Kleiner, M., Gordon, P.M.K., Pon, R.T., Dong, X., *et al*. (2019) A shared core microbiome in soda lakes separated by large distances. *Nat Commun* **10**: 4230. https://doi.org/10.1038/s41467-019-12195-5.

Supporting Information

Additional Supporting Information may be found in the online version of this article at the publisher's web-site:

Appendix S1: Data set. Numbers of metatranscriptomic reads mapping to the *Spiribacter halalkaliphilus* IM2438^T genome.

Fig. S1. Large-scale isolation of microorganisms from soda-saline lakes.

Fig. S2. Maximum-likelihood tree based on the 16S rRNA genes.

Fig. S3. Comparison of isoelectric point profiles of predicted proteomes.

Fig. S4. Sequence alignment of *c*-subunit of the F_1F_0-ATP synthases.

Fig. S5. Comparison of genome size and intergenic region median length.

Fig. S6. Exploring the effect of light on cell growth using different carbon sources.

Fig. S7. Time course of cell growth and lactate consumption in media of 20% salinity.

Fig. S8. Phylogenetic tree of sulfide: quinone oxidoreductase.

Fig. S9. Putative transmembrane region in the sulfide: quinone oxidoreductase of *Spiribacter halalkaliphilus* IM2438^T.

Fig. S10. Putative signal peptide region in the sulfide: quinone oxidoreductase of *Spiribacter halalkaliphilus* IM2438^T.

Table S1. Physiochemical parameters of samples used for microorganism isolation

Table S2. Composition of the media used in this article

Table S3. Culture conditions, habitats and taxonomy of isolates obtained in this article

Table S4. Sequence comparison of 16S rRNA genes between isolates and MAGs

Table S5. Representative isolates of nine MAGs based on the 16S rRNA gene

Table S6. Genome-level similarity analysis among *Spiribacter* species

Table S7. Summary for metatranscriptional sequencing and mapping against *Spiribacter halalkaliphilus*-encoding genes

Table S8. Functional genes and the relative transcriptional activity in four metatranscriptomes of natural brine samples

Table S9. Annotation of multicomponent Na^+:H^+ antiporter genes (*mnh*) in *Spiribacter* genomes

Table S10. Primers used in this study.